Available online at www.sciencedirect.com
ScienceDirect
Geochimica et Cosmochimica Acta 70 (2006) 4417–4435
Geochimica
www.elsevier.com/locate/gca

U–Sr isotopic speedometer: Fluid flow and chemical weathering rates in aquifers

Kate Maher [a,*], Donald J. DePaolo [a,b], John N. Christensen [b]

[a] Department of Earth and Planetary Science, University of California, Berkeley, CA 94720-4767, USA
[b] Earth Sciences Division, Lawrence Berkeley National Laboratory, 1 Cyclotron Road, Berkeley, CA 94720, USA

Received 27 December 2005; accepted in revised form 29 June 2006

Abstract

Both chemical weathering rates and fluid flow are difficult to measure in natural systems. However, these parameters are critical for understanding the hydrochemical evolution of aquifers, predicting the fate and transport of contaminants, and for water resources/water quality considerations. $^{87}Sr/^{86}Sr$ and ($^{234}U/^{238}U$) activity ratios are sensitive indicators of water–rock interaction, and thus provide a means of quantifying both flow and reactivity. The $^{87}Sr/^{86}Sr$ values in ground waters are controlled by the ratio of the dissolution rate to the flow rate. Similarly, the ($^{234}U/^{238}U$) ratio of natural ground waters is a balance between the flow rate and the dissolution of solids, and α-recoil loss of ^{234}U from the solids. By coupling these two isotope systems it is possible to constrain both the long-term (ca. 100's to 1000's of years) flow rate and bulk dissolution rate along the flow path. Previous estimates of the ratio of the dissolution rate to the infiltration flux from Sr isotopes ($^{87}Sr/^{86}Sr$) are combined with a model for ($^{234}U/^{238}U$) to constrain the infiltration flux and dissolution rate for a 70-m deep vadose zone core from Hanford, Washington. The coupled model for both ($^{234}U/^{238}U$) ratios and the $^{87}Sr/^{86}Sr$ data suggests an infiltration flux of 5 ± 2 mm/yr, and bulk silicate dissolution rates between $10^{-15.7}$ and $10^{-16.5}$ mol/m^2/s. The process of α-recoil enrichment, while primarily responsible for the observed variation in ($^{234}U/^{238}U$) of natural systems, is difficult to quantify. However, the rate of this process in natural systems affects the interpretation of most U-series data. Models for quantifying the α-recoil loss fraction based on geometric predictions, surface area constraints, and chemical methods are also presented. The agreement between the chemical and theoretical methods, such as direct measurement of ($^{234}U/^{238}U$) of the small grain size fraction and geometric calculations for that size fraction, is quite good.
Published by Elsevier Inc.

1. Introduction

U-series isotopes in natural waters provide a valuable means of quantifying chemical and physical weathering rates. Recent studies have used U-series isotopes to infer catchment scale erosion timescales (Vigier et al., 2001), the intensity of chemical weathering in regions of tectonic activity (Robinson et al., 2004), groundwater flow paths (Bonotto and Andrews, 2000; Luo et al., 2000; Reynolds et al., 2003), and *in situ* chemical weathering rates in aquifers and deep-sea sediments (Tricca et al., 2000, 2001; Maher et al., 2004). While other methods exist for calculating weathering rates *in situ*, few methods offer the distinct advantages presented by the U-series decay chain.

^{238}U is the principal isotope of natural uranium (99.72% abundance), while ^{234}U is a radiogenic daughter product in the ^{238}U decay chain (Dickin, 1995):

$$^{238}U(4.46\ Gy,\alpha) \rightarrow {}^{234}Th(24.1\ days,\beta\text{-}) \rightarrow {}^{234}Pa(1.18\ min,\alpha) \rightarrow {}^{234}U(248\ ky,\alpha).$$

In undisturbed rocks and minerals older than approximately 10^6 years the activity ratio of ($^{234}U/^{238}U$) is expected to be equal to one or "secular equilibrium" (where parentheses denote the activity ratio). The solid ($^{234}U/^{238}U$) ratio can depart from secular equilibrium as a result of the preferential release of ^{234}Th across grain boundaries via the recoil associated with the energetic α-decay of ^{238}U

* Corresponding author.
E-mail address: katem@eps.berkeley.edu (K. Maher).

0016-7037/$ - see front matter Published by Elsevier Inc.
doi:10.1016/j.gca.2006.06.1559

(4.1 MeV) (Krane, 1988; Ziegler et al., 1996). When decays occur proximal to the grain boundary, a substantial fraction of ^{234}Th can escape to the interstitial space where it likely decays to ^{234}U. By the processes of direct recoil ejection or leaching along recoil tracks, the surfaces of the mineral grains become depleted in ^{234}U and the surrounding interstitial pore fluids become enriched. Activity ratios as high as 11 have been observed in natural water (Porcelli and Swarzenski, 2003), while values as low as 0.5 have been measured in fine-grained sediments (Skwarzec, 1997; Skwarzec et al., 2002). Dissolution of the solids acts in opposition to the α-recoil effects by contributing U at the value in the solids, which is commonly $\leqslant 1$ for primary silicate minerals. Thus, the (^{234}U/^{238}U) ratio in pore water is a balance between the α-recoil of ^{234}Th, and weathering release of U from the sediments. If the rate of ^{234}U addition to the pore water via α-recoil can be determined, then the dissolution rate can be inferred from the (^{234}U/^{238}U) of the pore water.

The process of α-recoil of the ^{234}U nuclide from the solid to interstitial pore space is still relatively uninvestigated, despite the widespread conclusion that this process is largely responsible for the pronounced disequilibrium observed in natural waters. The fraction of daughter ^{234}U atoms that is lost from solid particles should depend on the ratio of the surface area to volume for the particle, and can be quite large for small, platy minerals. In natural sediments, heterogeneity in the grain size distribution complicates prediction of α-recoil loss because the smaller grains have a proportionally higher α-recoil loss fraction. Some measure of these microscopic, chemical and physical processes, which are extremely difficult to quantify in natural systems, and a predictive model to quantify these effects, is required to extract quantitative information from U-series data.

The α-recoil loss from silicate minerals has been calculated in a number of different ways, from geometric predictions based on mean grain size (Kigoshi, 1971; Tricca et al., 2000, 2001), fluid isotopic disequilibrium in Ra daughters (Krishnaswami et al., 1982; Luo et al., 2000; Porcelli and Swarzenski, 2003), measured (^{234}U/^{238}U) of sediment (Maher et al., 2004; DePaolo et al., 2006). These methods encompass either physical assumptions (grain size and grain geometry) or chemical observations. Grain sizes in natural sediments generally conform to a lognormal distribution, which implies that only a small mass-fraction of the sediment (typically the fraction $\leqslant 50$ μm in diameter) is contributing the bulk of the ^{234}U via α-recoil loss. Conversely, in fractured media, the surface area becomes the dominant control on the amount of α-recoil loss. Using natural samples of diverse grain size from sediments at the Hanford Site, Washington, several methods for quantifying the α-recoil loss from the solid can be compared.

The Hanford Site, in eastern Washington State is composed of sedimentary deposits ranging from 2 million year-old lacustrine deposits to younger (ca. 200,000 year-old) pre-Wisconsin cataclysmic flood deposits. The 70-m-thick vadose zone, composed of sediments similar in mineralogy, affords an opportunity to investigate the processes of α-recoil loss. Here, we compare methods for calculating α-recoil loss in the context of quantifying infiltration rates and chemical weathering. Because the pore water activity ratio is a function of the α-recoil flux, the dissolution of bulk solids, and the infiltration flux, additional information is required to arrive at an estimate of either the bulk dissolution rate or the infiltration rate. Here, we use previous estimates of the ratio of the dissolution rate to the infiltration flux based on Sr isotopes (Maher et al., 2003) to arrive at a coupled U–Sr model for determining *in situ* rates of dissolution and infiltration.

2. Site description

The Hanford/DOE Site in eastern Washington State is located within the arid Pasco Basin, a broad structural depression within the Columbia Plateau (Fig. 1). The basin is underlain by Miocene-age flood basalts from the Columbia River Basalt Group. Overlying the flood basalts are extensive fluvial, pedogenic, lacustrine, and eolian deposits of Miocene to Holocene age (Lindsey et al., 1994; USDOE, 2002).

Substantial amounts of radioactive waste material have been disposed into the surface soils and vadose zone at Hanford Site. Borehole 299-W22-48 (71.6 m) was drilled in the 200 West area in order to characterize the back-

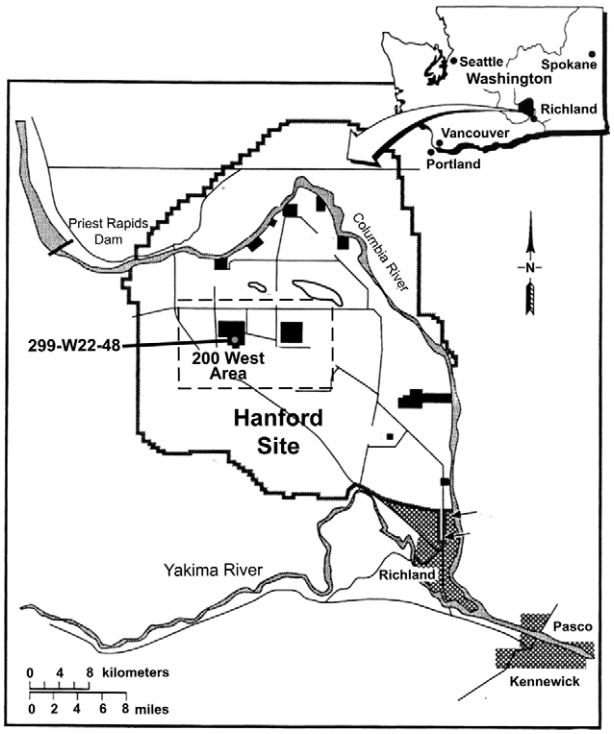

Fig. 1. Hanford Site map showing location of the 200 Area plateau and the 299-W22-48 bore hole and other pertinent locations. The nuclear reactors (black rectangles) were located adjacent to the Columbia River. The majority of the chemical processing occurred in the 200 Areas (stippled box).

ground geochemistry and the geology of the area proximal to contaminated zones. The volumetric water content (θ) and corresponding lithology (measured by Serne et al. (2002)) are shown in Fig. 2. The upper Hanford Formation is composed of gravel-to-silt size sediments deposited by a series of Pleistocene cataclysmic glacial floods. The youngest of these flood deposits was emplaced at ~15 ka (Lindsey et al., 1994). Sand and silt-dominated facies comprise the lower sand-dominated Hanford Formation sediments (HFSD2). At the base of the Hanford Formation deposits is the early-Pleistocene to late Pliocene Cold Creek unit (CCU) composed of alluvial and pedogenic deposits. The upper lithofacies of the Cold Creek unit, CCUf(lam-msv) is a fine-grained laminated fluvial deposit. The CCUc-f(calc) is a fine-to-coarse grained, calcium-cemented paleosol with approximately 40 weight percent $CaCO_3$ (USDOE, 2002). The low permeability of the CCU strongly affects movement of water through the vadose zone. The late Miocene to early-Pliocene Ringold Formation (3.4–8.5 Ma) consists of variably cemented clay, silt, sand, and pebble to cobble-size gravel of fluvial or lacustrine origin.

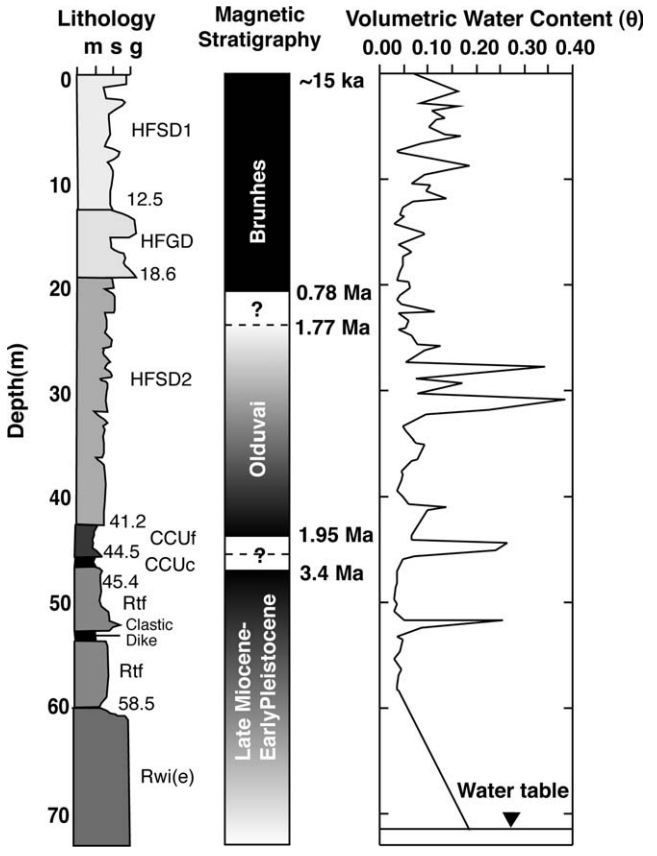

Fig. 2. Lithology and volumetric water content (θ) for the 299-W22-48 borehole. HFGD, Hanford Formation, gravel-dominated facies; HFSD, Hanford Formation, sand-dominated facies; CCUf(lam-msv), cold Creek unit, silt and fine-grained sand; CCUc-f(calc), Cold Creek unit, calcic paleosol; Rtf, Ringold Formation, upper fines; Rwi, Ringold Formation, sandy gravel. The approximate sedimentary age of the deposits is shown for reference. Black shading indicates normal magnetic polarity, white reversed, and gray is unconstrained with dashed lines representing the approximate location. Data from Serne et al. (2002), USDOE (2002) and Bjornstad et al. (2001).

Gravimetric water contents were converted to volumetric water content assuming a constant bulk density of 1.9 g/cm^3. The average water content of the sediments is 9% by volume, but varies from 3% to 39%. The water content is notably elevated at 26–32 m depth in the HFSD2 Formation, at 44.5 m in the CCUf unit above the calcic paleosol, and at 52 m corresponding to a clastic dike in the Ringold Formation. There is close correspondence between the elevated water content and the finer-grained units.

The sediments are predominantly composed of quartz, plagioclase, alkali feldspar, and minor accessory minerals such as biotite, calcite, and clays (Serne et al., 2002; Maher et al., 2003). The most notably different layer is the lower Cold Creek unit (CCUc-f(calc)), which has a high calcite content (40%). Major element chemistry was also measured. However, the profiles show no systematic change with depth which is common in young unconsolidated weathering profiles. Speciation calculations using EQ3/EQ6 (Wolery et al., 1990) suggest that the pore waters are undersaturated with respect to plagioclase and K-feldspar, and saturated with respect to calcite throughout the profile. Attempts were made to model the profiles using a standard reactive transport approach similar to Maher et al. (2006), however the problem of evaporation and lack of quantitative mineralogy hindered these efforts.

The grain size distributions were also measured as part of the initial core characterization and are tabulated in Serne et al. (2002). The upper HFSD1 facies of the Hanford Formation is composed predominantly of sand (~90%) and inter-bedded silt and clay layers (~8%) with slightly higher water contents (Table 1, Fig. 2). The gravel-dominated HFGD unit is the coarsest in composition, ranging from 63.2% gravel and 36% sand, to 3% gravel and 92% sand at the contact with the finer-grained lower HFSD2 unit (94–98% sand). The silt and clay contents were highest in the Cold Creek units (38.6%), whereas the Ringold Formation is predominantly sand and silt (Serne et al., 2002).

3. Analytical procedures

3.1. Surface area measurements

BET (Brunauer–Emmett–Teller) surface areas were measured by N_2 gas adsorption for selected depths from the 299-W22-48 borehole. The first measurements were performed on fresh dry sediment. Subsequent measurements were performed on the same samples after leaching in 8 N HNO_3 to determine the effect of strong acid leaching on the surface structure of the minerals (Table 1).

3.2. Sequential leaches

As a result of the low water content and deep vadose zone (ca. 70 m) at the Hanford Site, deionized water leach-

Table 1
Particle size distribution and BET Surface area from untreated bulk sediment and for sediment after leaching in 8 N HNO_3

Depth (m)	Unit	Surface area[a]			Gravel (%)	Sand (%)	Silt (%)	Clay (%)	Calcite (%)
		Bulk (m^2/g)	After leach (m^2/g)	Geo (m^2/g)[b]					
12.0	HFSD1	5.2	10.2	0.37	0.2	77.6	20.6	1.7	1.8
14.3	HFGD	3.7[c]	4.8[c]	0.36	64.6	18.7	15.1	1.5	1.3
27.9	HFSD2	—	—	0.55	0.3	70.6	27.	2.1	1.8
30.9	HFSD2	7.3[d]	22.7[d]	0.39	0	78.7	18.8	2.5	3.3
41.5	CCUf	78.8	28.7	1.33	0.01	18.5	75.9	5.6	2.9
44.5	CCUc-f	—	—	0.30	52.4	27.1	15.2	5.3	38.3
49.8	Rtf	4.4	10.4	0.33	0.01	89.0	9.7	1.3	0.75

Particle size distributions determined by wet sieve/hydrometer methods [data summarized from Serne et al. (2002)].
[a] In some cases corresponding samples could not be obtained for BET surface area measurements, so the nearest sample is shown for comparison.
[b] Calculated from gain size distributions using the wt fraction and median particle diameter for each interval.
[c] 15.3 m depth.
[d] 29.4 m depth.

es were used to extract the pore water solutes. Leach procedures were used to extract information about the chemical and isotopic character of the sediments. The leach procedure is as follows:

1. *Pore water:* 1:1 sediment to de-ionized water leaches were prepared using 50 g of dry sediment and 50 mL of 18 MΩ de-ionized water. The leaches were placed in an ultrasonic bath for 90 min and allowed to stand for 24 h. The mixture was then vacuum filtered through a 0.45 μm polyethylene filter into screw-top polyethylene bottles. The uranium contained in the rinse water is assumed to be that which was originally dissolved in the pore fluid, plus any readily exchangeable uranium on the solid phases. The theoretical U concentration for the pore waters was calculated using the water content data and a bulk density of 1.9 g/cm^3.
2. *Authigenic $CaCO_3$:* The carbonate fraction of the sediments was extracted following the procedure of Tessier et al. (1979) with slight modifications. After leaching in de-ionized water, 8 g of dry sediment was mixed with 15 ml of 1 M NaOAc (adjusted to pH 5 with acetic acid) for 5 h. The solutions were filtered as described above and dried prior to chemical separation of the uranium.
3. *Nitric acid dissolvable fraction:* Strong nitric acid (HNO_3) leaches were performed on dry splits from the de-ionized leach procedure. For the nitric acid leaches, 5 g of sediment were combined with 15 ml of double-distilled 8 N nitric acid and heated for 6–8 h at 70 °C then allowed to cool overnight before filtering. For purposes of inter-laboratory comparison with measurements performed at Pacific Northwest laboratory (PNNL), nitric acid leaches were performed on samples previously treated with only distilled water, thus these HNO_3 leaches contain some $CaCO_3$.
4. *Bulk sediment/size fractions:* Uranium concentrations for the bulk sediment and size fraction separates were measured for 100–300 mg splits dissolved in a mixture of concentrated perchloric and hydrofluoric acids. After heating for 48 h on a hot plate, the solution was evaporated to dryness and re-dissolved in 1.5 N HNO_3 prior to the chemical separations. (Bulk sediment U concentrations were also measured by XRF methods in Serne et al. (2002), and were generally below the detection limit of 6 ppm). Different methods of sample pre-treatment were considered in order to ensure that secondary minerals were removed prior to digestion of the sediment for U isotopic analysis. This included (i) dissolution with no sample pre-treatment; (ii) leaching for 1 h in 1 N NaOAc, followed by two rinses in deionized water; and (iii) leaching for 30 min in 1 N hydrochloric acid (HCl) in an ultrasonic shaker, followed by two rinses in deionized water. The samples were centrifuged for 20 min and the supernatant removed between each rinse step.

3.3. Grain size fractions/mineralogy

Grain size separates for bulk U analysis were created using standard USGS Teflon micro-sieves (45, 60, 75 and 600 μm). Fresh air-dry samples were used. Because the Hanford sediments are predominately sand, and are not cemented (except for the Cold Creek Units), no further sample manipulation was performed prior to sieving.

3.4. Isotopic analyses

All U samples (water, NaOAc leachates, acid, bulk sediment digestions, etc.) were purified by ion exchange chromatography using Eichrom TRU-spec resin in 0.2 ml Teflon columns following the procedure of Luo et al. (1997). Yields for the chemical separations are about 90–95%. All U isotopic ratios were measured on a Micromass IsoProbe multiple collector ICP source magnetic sector mass spectrometer (MC-ICPMS) at LBNL (Lawrence Berkeley National Laboratory). This instrument is equipped with nine movable Faraday cups, two movable channeltron electron multipliers, and an axial Daly photo multiplier ion counting system. Corrections for mass fractionation were conducted internally using measured $^{235}U/^{238}U$ of the sample, while Daly–Faraday inter-calibration was calculated from bracketed analyses of an in-house

secular equilibrium natural uranium standard as described in Christensen et al. (2004). U concentrations for samples were calculated by comparing the sample ^{238}U intensity to that of the 20 ppb U standards.

4. Results

4.1. (^{234}U / ^{238}U) in pore waters and leaches

The U isotopic and concentration profiles for the pore water, nitric acid leaches and NaOAc leaches are shown in Figs. 3 and 4. The pore water ($^{234}U/^{238}U$) ratios increase with depth from values of 1.03 to 1.05 at the surface to a value of 1.21 at 54 m depth (Table 2). The deepest sample is below the water table within the unconfined aquifer and has the highest ($^{234}U/^{238}U$) of 1.24. The pore water samples from the carbonate-rich paleosol units (CCUf and CCUc) and the upper Ringold have distinctly lower ($^{234}U/^{238}U$) values of 1.05–1.06, and high U concentrations (90–100 μg/L). Beneath the Cold Creek Unit, the pore water values increase again from an initial value of 1.04 in the upper-most Ringold Formation (49.8 m). The ($^{234}U/^{238}U$) of the remaining samples in the lower Ringold Formation increase with approximately the same linear trend of increasing values observed in the upper 45 m. There is no correlation between the U isotopic ratios and water content. The NaOAc leachate ($^{234}U/^{238}U$), which should represent the carbonate fraction of the sediment, are similar to the pore water ($^{234}U/^{238}U$) (Tables 3 and 2). However, for the samples between 15 and 21 m the ($^{234}U/^{238}U$) of the NaOAc leaches are significantly higher than those of the pore water.

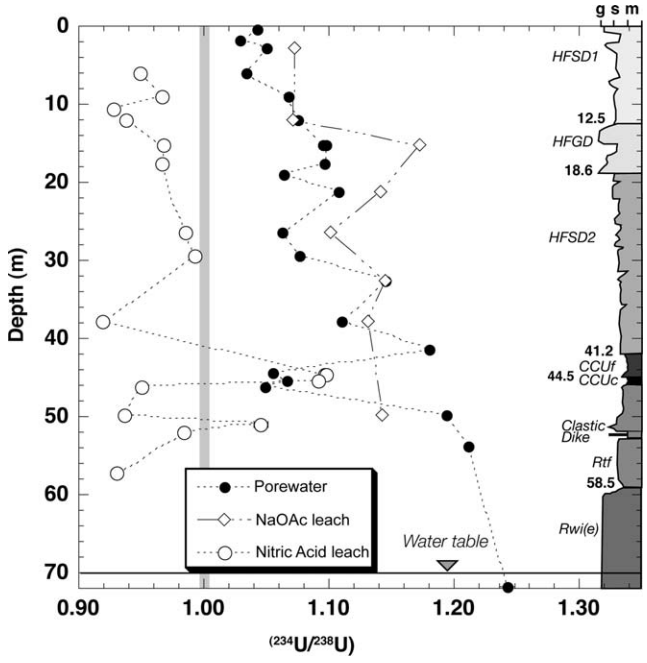

Fig. 3. ($^{234}U/^{238}U$) ratios for nitric acid, NaOAc and pore water leaches. The stratigraphic column and the depth of the contacts are shown for reference.

The 8 N HNO_3 dissolves uranium that is depleted in ^{234}U relative to secular equilibrium (Fig. 3, Table 4). The data show considerable variation between activity ratios of 0.92–0.96 in the upper sand-dominated Hanford Formation (HFSD1) and in the deeper Ringold sediments, to higher values of 0.96–0.97 in the coarser-grained gravel-dominated units of the Hanford Formation (HFGD). The notable exceptions are the samples from the Cold Creek units, which are primarily $CaCO_3$. These samples have ($^{234}U/^{238}U$) ratios that are greater than the pore water values from this part of the core.

In general, the concentration estimates from the pore water and nitric acid leach procedures performed here agree well with the values from identical leach procedures measured by ICP-MS and reported in Serne et al. (2002). There is little variation in the U concentrations with depth, excluding the pore waters of the CCU, which have elevated U concentrations (Fig. 4). The U concentrations from the nitric acid leach in these units are also quite high (4 μg/g sediment) compared to average values of approximately 0.44 μg/g sediment for the rest of the profile.

The nitric acid leach presumably also dissolved secondary carbonate. The ($^{234}U/^{238}U$) values of the carbonate reflect the composition of the pore water over time, and are thus substantially different than the bulk rock values. The sediments contain on average about 2 wt% $CaCO_3$ (Serne et al., 2002). Assuming the NaOAc leach completely dissolved all of the calcite, we estimate calcite uranium concentrations between 0.2 and 0.9 ppm. The nitric acid leach ($^{234}U/^{238}U$) values on a carbonate-free basis can be estimated from the data using the wt% $CaCO_3$ from Serne et al. (2002) and the measured U in the NaOAc leaches (Tables 3 and 4). Assuming a concentration of 1 ppm U in the calcite, the ($^{234}U/^{238}U$) nitric acid values would be approximately 0.2% (6, 49.8 m) to 1% (37.9 m) lower than measured, with an average decrease of 0.7%. Given our best estimate of the U concentrations in the carbonate (<1.0 ppm), the dissolution of small amounts of secondary carbonate affects the ($^{234}U/^{238}U$) value of the nitric acid leach by no more than 1%. Thus, the ($^{234}U/^{238}U$) nitric acid values represent a maximum value for the depleted reservoir. In systems with high amounts of secondary minerals the effect would be much more significant, and further sample pre-treatment would be necessary.

4.2. ($^{234}U/^{238}U$) in bulk sediment and grain size fractions

A summary of the data for the grain size fractions and bulk solids is shown in Tables 5a and 5b and Fig. 5. The results of two methods employed to remove secondary minerals (1 N NaOAc and 1 N HCl) are also shown. The <45 μm fraction (fresh samples) is in general depleted in ^{234}U relative to the secular equilibrium value, the bulk solids and the larger grain sizes (Tables 5a and 5b). The untreated samples from HFSD1 have the lowest

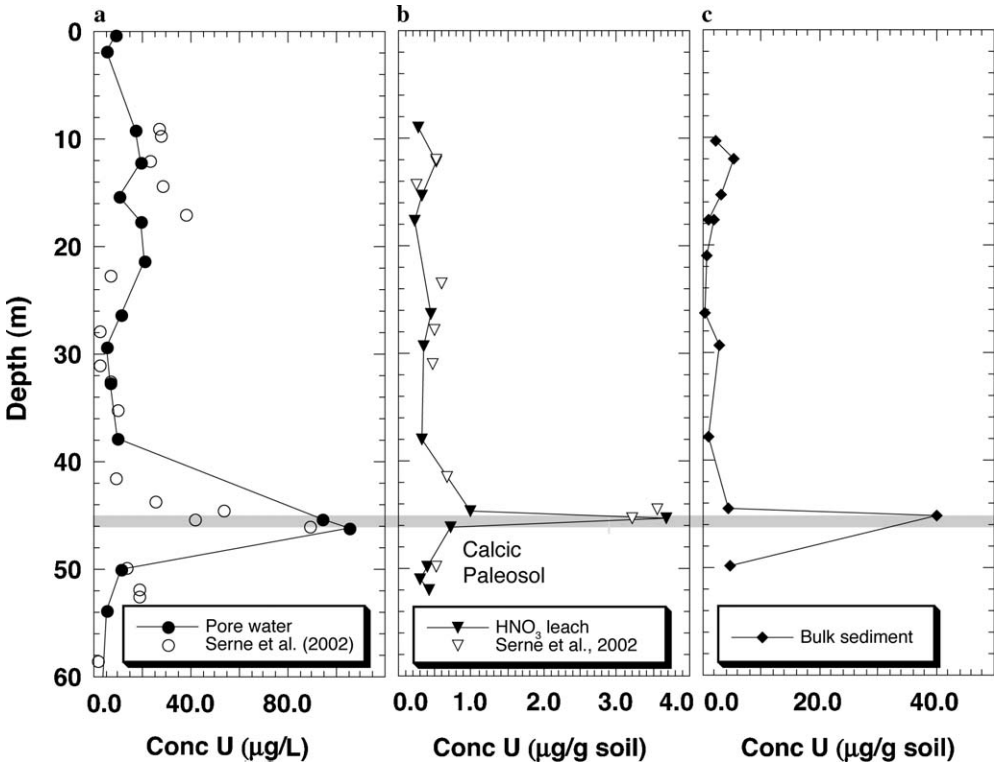

Fig. 4. (a) Pore water, (b) nitric acid leach and (c) bulk sediment uranium concentrations compared to measurements from Serne et al. (2002). Nitric acid leach uranium concentrations are not on a carbonate-free basis, therefore the large peak in the calcic paleosol unit is attributed to the dissolution of $CaCO_3$.

($^{234}U/^{238}U$). The ($^{234}U/^{238}U$) ratios increase in the coarser-grained HFGD unit (12–18 m) and in the HFSD2 unit, then decrease again in part of HFSD2 and the Ringold Formation (Rtf). The values range from approximately 0.94 to 0.99. Given the different depositional facies within the borehole, the variation in ($^{234}U/^{238}U$) is most likely related to the grain size distributions. This trend is similar to that observed in the nitric acid leaches—in the coarser-grained units, the majority of the grain sizes in the <45 μm fraction are distributed towards the upper-end of the 45 μm range where the α-recoil loss fraction is expected to be lower.

There are substantial differences between the samples that were not pre-treated, and the samples that were leached prior to digestion. In general the ($^{234}U/^{238}U$) values for all treatments are higher in the HFGD and upper part of the HFSD2, and then decrease below 30 m depth. The difference between the ($^{234}U/^{238}U$) measured on NaOAc leachates and untreated samples is largest in the shallowest samples.

The lowest ($^{234}U/^{238}U$) values were measured for samples that had no pre-treatment step. This could be due to several factors, namely: (i) centrifuging between rinses resulted in loss of the finest-grained, and therefore the most depleted grains within the <45 μm fraction, and (ii) leach procedures may have dissolved some of the depleted surface materials. For the present purposes, we will assume that the <45 μm fraction is best represented by the samples which were not pre-treated. These samples may contain some secondary carbonate that may have increased the activity ratio by about 1%.

5. Discussion

5.1. Interpretive model of U isotopes in pore fluid

Solute transport and chemical weathering rates in aquifers are known to be closely linked (Stonestrom et al., 1998; White et al., 2005). However, in practice it is very difficult to measure these parameters in the field. Coupling isotopes that are sensitive to water–rock interaction such as Sr and U provides a means of quantifying both the infiltration flux and the dissolution rate, and may thus serve as an isotopic speedometer for the hydrochemical character of a weathering profile.

The isotopic composition of uranium in the vadose zone is controlled by a balance between fluid flow, weathering of the bulk sediment and the α-recoil of ^{234}U (via ^{234}Th) to the sediment. In arid vadose zones, secondary mineral precipitation often occurs as well. We assume that secondary minerals incorporate U with the ($^{234}U/^{238}U$) of the fluid, therefore the pore water isotopic composition is not affected by precipitation of carbonate (or any other authigenic phase). However, the incorporation of U into secondary minerals does affect the total concentration of U in the pore water.

Sr and U isotopic models of water–rock interaction have been proposed for a multitude of diverse hydrologic trans-

Table 2
Uranium data for 1:1 deionized water leaches

Depth (m)	Volumetric water content (θ)	1:1 Water extract ($^{234}U/^{238}U$)[a]	Apparent U concentration[c]: (μg/L)[d]
0.4	0.094	1.0427 ± 0.0024	8.7
1.9	0.177	1.0293 ± 0.0011	5.2
2.9	0.168	1.0499 ± 0.0023	
6.0	0.134	1.0341 ± 0.0016	
9.0	0.172	1.0673 ± 0.0017	17.0
12.0	0.124	1.0748 ± 0.0011	19.1
15.3	0.094	1.0953 ± 0.0017	10.5
15.3	0.094	1.0970 ± 0.0013	15.7
17.6	0.060	1.0965 ± 0.0012	19.7
19.0	0.049[b]	1.0634 ± 0.0026	
21.3	0.034	1.1077 ± 0.0015	21.1
26.4	0.096	1.0622 ± 0.0017	11.1
29.4	0.209	1.0759 ± 0.0018	5.3
32.6	0.061	1.1453 ± 0.0018	6.9
37.9	0.069	1.1098 ± 0.0013	9.7
41.5	0.108[b]	1.1806 ± 0.0024	
44.5	0.430	1.0548 ± 0.0011	
45.2	0.178	1.0658 ± 0.0011	94.0
46.2	0.038	1.0484[e] ± 0.0014	104.9
49.8	0.036[b]	1.1940 ± 0.0018	11.0
53.8	0.094[b]	1.2119 ± 0.0022	5.3
71.8	0.253	1.2425 ± 0.0065	0.2

[a] Errors are 2σ.
[b] Data from Serne et al. (2002).
[c] Apparent U concentration derived by normalizing ^{238}U beam intensity from the sample to that of the standard analyses bracketing the sample. This concentration does not account for U lost during chemical separation and the differences in the ion beam focusing. In some cases concentrations were not calculated because of variation in the standard beam intensity.
[d] Concentrations of theoretical pore waters were calculated using the water content data and a bulk density of 1.9 g/cm^3.
[e] Average of six samples from this depth: 1.0486 ± 0.001; 1.0495 ± 0.0012; 1.0473 ± .0010; 1.0474 ± 0013; 1.0494 ± 0.0013; and 1.0484 ± 0.0013.

Table 3
NaOAc leachate data

Depth (m)	$(^{234}U/^{238}U)_{Act}$[a]	U (ng/g soil)[b]
2.9	1.0726 ± 0.0016	14.14
12.0	1.0709 ± 0.0016	5.10
15.3	1.1720 ± 0.0013	16.87
21.3	1.1413 ± 0.0014	18.02
26.4	1.1012 ± 0.0013	3.73
32.6	1.1449 ± 0.0013	17.21
37.9	1.1313 ± 0.0025	4.47
49.8	1.1426 ± 0.0025	7.42

[a] Errors are 2σ.
[b] Apparent U concentration derived by normalizing ^{238}U beam intensity to that of the standard analyses bracketing the sample. This concentration does not account for U lost during chemical separation and the differences in the ion beam focusing. In some cases concentrations were not calculated because of variation in the standard beam intensity.

Table 4
U data from 8 N nitric acid leaches

Depth (m)	$(^{234}U/^{238}U)$[a]	U (μg/g soil)[b]
6.0	0.9490 ± 0.0014	
9.0	0.9665 ± 0.0019	0.277
10.6	0.9278 ± 0.0014	
12.0	0.9376 ± 0.0013	0.513[c]
15.3	0.9677 ± 0.0014	0.332
17.6	0.9668 ± 0.0014	0.230
26.4	0.9851 ± 0.0019	0.434
29.4	0.9926 ± 0.0021	0.347
37.9	0.9190 ± 0.0014	0.321
44.5	1.0959 ± 0.0021	0.990
44.5	1.0970 ± 0.0021	0.980
45.2	1.0911 ± 0.0015	3.681
46.2	0.9505 ± 0.0017	0.710
49.8	0.9368 ± 0.0019	0.400
51.1	1.0453 ± 0.0055	0.285
52.0	0.9842 ± 0.0012	0.428
57.2	0.9301 ± 0.0011	

[a] Errors are 2σ.
[b] Apparent U concentration (see footnote a, Table 3).
[c] Data from equivalent 8 N nitric acid leach reported in Serne et al. (2002).

Table 5a
$^{234}U/^{238}U$ activity ratios and U concentrations for the bulk solid

Depth (m)	Formation	Whole rock/minerals ($^{234}U/^{238}U$)	U Conc. (μg/g)
10.4	HFSD	1.000[a] ± 0.0023	
10.4	HFSD	0.979 ± 0.0014	2.04
12.0	HFSD	0.997 ± 0.0016	5.15
15.3	HFGD	0.995 ± 0.0009	3.17
17.6	HFGD	0.985 ± 0.0010	0.90
17.6	HFGD	1.017 ± 0.0066	1.78
21.0	HFSD2	1.066[b] ± 0.0013	0.51
26.4	HFSD2	0.992 ± 0.0019	0.38
29.4	HFSD2	0.988 ± 0.0019	2.72
37.9	HFSD2	1.004 ± 0.0019	1.09
44.5	CCUf	1.062 ± 0.0016	4.47
45.1	CCUc	1.080 ± 0.0022	40.2
49.8	Rtf	0.972 ± 0.0033	4.52

[a] K-feldspar mineral separate.
[b] Biotite mineral separate.

port regimes such as fractured groundwater systems (Krishnaswami et al., 1982; Ku et al., 1992; Johnson and DePaolo, 1994, 1997; Luo et al., 2000), sandy aquifers (Tricca et al., 2001), and ocean sediments (Richter and Liang, 1993; Maher et al., 2004). The model presented here is adapted from these previous models to treat vadose zone water–rock interactions and the associated processes for U isotopes.

The general transport equation for ^{234}U in the vadose zone, including the processes of α-recoil (R_α), dissolution of solid phases (R_d), decay (λ), adsorption (K_r), and removal of uranium by precipitation of authigenic minerals (R_p) is given by

$$K_{r,234}\frac{\partial C_{f,234}}{\partial t} = \frac{\partial}{\partial z}\left(D_e\frac{\partial C_{f,234}}{\partial z}\right) - v\frac{\partial C_{f,234}}{\partial z} + R_\alpha + R_d - R_p + \lambda_{238}C_{238}K_{r,238} - \lambda_{234}C_{f,234}K_{r,234}, \quad (1)$$

where $C_{f,234}$ is the aqueous concentration of ^{234}U, K_r is an isotopic retardation coefficient (Table 6), and D_e and v correspond to the dispersion coefficient and advective velocity.

Table 5b
$^{234}U/^{238}U$ activity ratios for the <45 μm and 45–60 μm size fractions for the three different methods of sample pretreatment (errors are 2σ)

Depth (m)	Unit	<45 μm fraction			45–60 μm fraction
		($^{234}U/^{238}U$) (no pre-treatment)	($^{234}U/^{238}U$) (HCl leach)[b]	($^{234}U/^{238}U$) (NaOAC leach)[c]	($^{234}U/^{238}U$) 45–60 μm[d]
0.3	HFSD	0.9670 ± 0.0022	1.0105 ± 0.0016		0.9993 ± 0.0011
1.8	HFSD	0.9644 ± 0.0015	0.9986 ± 0.0016		
2.9	HFSD	0.9639 ± 0.0014			
6.0	HFSD	0.9471 ± 0.0016	1.0089 ± 0.0015		
8.8	HFSD	0.9473 ± 0.0012	0.9768 ± 0.0016		
12.0	HFSD	0.9885 ± 0.0017			
15.3	HFSD	1.0032 ± 0.0014		1.0124 ± 0.0022	1.0050 ± 0.0018
17.6	HFGD	0.9846[a] ± 0.0087	0.9983 ± 0.0017	1.0091 ± 0.0022	
21.0	HFSD2	0.9831 ± 0.0017	0.9893 ± 0.0017	0.9998 ± 0.0023	0.9626 ± 0.0015
26.4	HFSD2	0.9907[a] ± 0.0019		1.0002 ± 0.0020	
29.4	HFSD2			1.0026 ± 0.0020	0.9881[a] ± 0.0017
32.3	HFSD2			0.9928 ± 0.0020	
37.9	HFSD2		0.9789 ± 0.0021	0.9725 ± 0.0024	
44.5	CCUf	1.0546[a] ± 0.0016			1.0620 ± 0.0019
46.2	CCUc	0.9607[a] ± 0.0020	0.9634[a] ± 0.0137	0.9472 ± 0.0025	
49.8	Rtf	0.9762 ± 0.0015	0.9880[a] ± 0.0054	0.9639 ± 0.0024	
53.6	Rtf		0.9496 ± 0.0023	0.9571 ± 0.0022	

[a] Average of duplicate samples.
[b] Samples leached in 1.5 N HCl for 30 min in ultrasonic shaker.
[c] Samples leached in 1.0 N NaOAc for 5 h.
[d] Samples with no pretreatment prior to dissolution, larger grain-size fraction (45–60 μm).

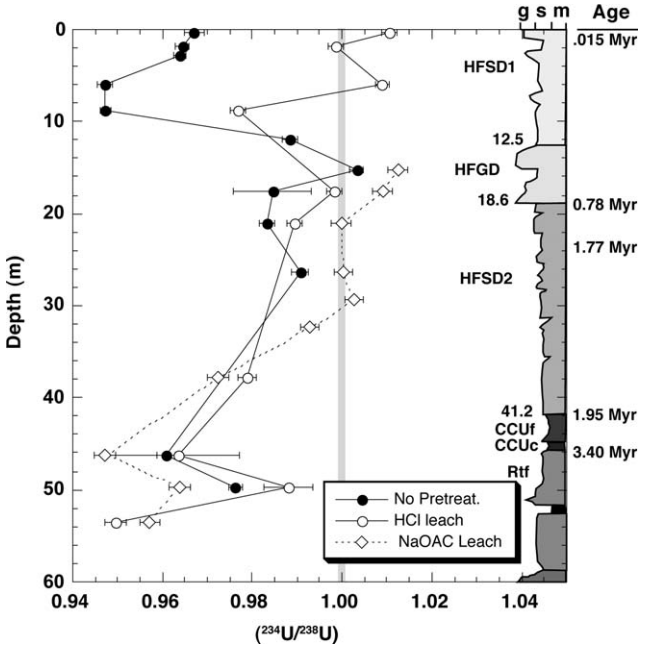

Fig. 5. ($^{234}U/^{238}U$) values for solid fractions <45 μm in diameter for three different leach procedures.

All parameters, units and assumed values are also defined in Table 6.

The α-recoil term is equal to

$$R_\alpha = M_s f_\alpha(S, d_p)\lambda_{238} C_{s,238}, \tag{2}$$

where f_α is the fraction of ^{238}U decays which result in direct injection of the ^{234}Th nuclide into the pore water and depends on the specific surface area (S) and grain size (d_p) of the material. M_s is the mass of solid per volume fluid, and C_s is the concentration of U in the solid. The overall α-recoil flux is dependent on both the f_α parameter, and the concentration of U in the solid. To quantify f_α requires a detailed analysis of the solids.

The dissolution term is defined as

$$R_d = \sum_i M_{s,i} k_{f,i} S_i C_{s,i}, \tag{3}$$

where k_f is the mineral dissolution rate constant, $C_{s,i}$, is the concentration of U in the mineral, S_i is the specific surface area of the mineral. The precipitation term is similarly defined as

$$R_p = M_s k_p K_s C_f, \tag{4}$$

where k_p is the bulk precipitation time constant, and K_s is the equilibrium precipitation constant, which is defined as the ratio of the concentration of U in the solid to the fluid.

The equation for ^{238}U is similar to that of ^{234}U, except the R_α term is absent and the decay terms are modified:

$$K_{r,238}\frac{\partial C_{f,238}}{\partial t} = \frac{\partial}{\partial z}\left(D_e \frac{\partial C_{f,238}}{\partial z}\right) - v\frac{\partial C_{f,238}}{\partial z} + \sum_i M_{s,i} k_{f,i} S_i C_{s,238,i} - M_{s,j} k_{p,j} S_j K_s C_{f,238} - \lambda_{238} K_{r,238} C_{f,238}. \tag{5}$$

Eqs. (1) and (5) can be combined to express the ($^{234}U/^{238}U$) ratio using the chain rule:

$$K_r\frac{\partial A_f}{\partial t} = D_e\frac{\partial^2 A_f}{\partial z^2} - v\frac{\partial A_f}{\partial z} + \sum_i \frac{M_{s,i} C_{s,i} k_{f,i} S_i}{C_f}[A_s - A_f] + \frac{M_s f_a \lambda_{234} C_s}{C_f} + K_r\lambda_{234}[1 - A_f]. \tag{6}$$

Table 6
Equation parameters and estimated values for Hanford sediments

Parameter	Description	Units (or values)
A_f	($^{234}U/^{238}U$) activity ratio in pore fluid	
A_s	($^{234}U/^{238}U$) activity ratio in solid phase	
C_e	Concentration of U in adsorbed phase per total volume	atoms/cm^3-total
C_f	Concentration of U in solution	atoms/cm^3-fluid
C_s	Concentration of U in solid phase	atoms/g-solid
D_e	Dispersion coefficient, including hydrodynamic dispersivity and molecular diffusion.	0.031 m^2/yr
f_α	α-recoil loss factor	
F_α	Weighted geometric α-recoil loss factor	
K_r	Retardation factor for uranium ($=1 + C_e/\theta C_f$)	<1 to 4
K_s	Equilibrium distribution coefficient for precipitated solids	C_s/C_f
k_f	Surface–area normalized dissolution rate constant	mol/m^2/s
k_p	Time constant for precipitation	yr^{-1}
λ_i	Decay constant for ^{234}U or ^{238}U[a]	yr^{-1}
λ_r	Surface roughness factor (ratio of measured to geometric surface areas)	
L	α-recoil length	300 Å/0.03 μm
M_s	Solid mass to fluid volume ratio	g/cm^3 fluid
MW	Molecular weight of feldspar	270 g/mol
θ	Volumetric water content	cm^3/cm^3
q	Infiltration flux ($=v\theta$)	mm/yr
ρ_b, ρ_m	Bulk density/mineral density	1.9/2.7 g/cm^3
ρ_f	Fluid density	g/cm^3
r_i	$^{234}U/^{238}U$ or $^{87}Sr/^{86}Sr$ atomic ratio for phase i (solid, fluid, etc.)	
R_d	Weathering rate	atoms/cm^3/yr
R_p	Precipitation rate of secondary minerals	atoms/cm^3/yr
R_α	α-Recoil loss rate	atoms/cm^3/yr
S	Specific surface area	m^2/g
v_f	Fluid velocity	mm/yr
z	Depth coordinate in sediment (increasing downward)	m

[a] $\lambda_{234} = 2.83 \times 10^{-6}$ yr^{-1}, $\lambda_{238} = 1.55 \times 10^{-10}$ yr^{-1} (Jaffey et al., 1971; Cheng et al., 2000).

The major assumptions in this formulation are that (i) the concentration of ^{238}U is equal to the concentration of total uranium, (ii) the isotopic retardation factors are equivalent for both ^{234}U and ^{238}U, (iii) reversible exchange (e.g. ^{234}U produced from adsorbed ^{234}Th is partitioned according to the distribution coefficient for U), (iv) the ($^{234}U/^{238}U$) of the precipitating solid is equal to that of the pore fluid at the time of precipitation, and (v) $\lambda_{238} - \lambda_{234} = -\lambda_{234}$. Eq. (6) can be simplified by considering the length scales over which different aspects of the system operate (Johnson and DePaolo, 1994, 1997; Maher et al., 2004). Reactive length scales describe the distance over which the pore fluid signal responds to the processes of dissolution and transport. The length scale for dispersive transport in the vadose zone is given by Eq. (7a), and the length scale for is advective transport given by Eq. (7b):

$$\mathrm{Ld}_U = \left(\frac{D_e}{Sk_f M_s C_s/C_f}\right)^{1/2}, \tag{7a}$$

$$\mathrm{La}_U = \left(\frac{q}{\theta M_s C_s/C_f S k_f}\right). \tag{7b}$$

The value of $M_s C_s/C_f$ in the Hanford pore waters averages 6000. For an infiltration flux ($q = v\theta$) of 7 mm/yr and a bulk dissolution rate (Sk_f) of $\sim 10^{-6.5}$ yr^{-1} (Maher et al., 2003), a water content (θ) of 0.09, and a dispersion coefficient (D_e) of 0.03 m^2/yr (based on a dispersivity of 0.4 m, Kincaid et al., 1998), the advective length scale is ~40 m, compared to ~4 m for the dispersive length scale. The relatively long length scale for advection in the Hanford sediment implies that in this system, advection has an important effect on the observed isotope ratios.

At steady state, assuming that dispersion is negligible in comparison to the reaction rate term, Eq. (6) can be reduced to

$$\frac{\partial A_f}{\partial z} = \frac{\theta M_s S_i k_{f,i} C_s}{q C_f}(A_s - A_f) + \frac{\lambda_{234}}{q}\left(\frac{\theta M_s f_\alpha C_s}{C_f}\right) + \frac{\theta K_r \lambda_{234}}{q}(1 - A_f). \tag{8}$$

The activity of the fluid is thus a function of the α-recoil loss fraction, the infiltration flux, and the weathering rate. These dependencies are evident in Fig. 4, where the pore water values increase with depth. A relative increase in weathering or dissolution would effectively lower the ($^{234}U/^{238}U$) of the fluid, while an increase in the α-recoil loss would increase the fluid ($^{234}U/^{238}U$) values.

This formulation assumes diffuse meteoric recharge through the unsaturated zone and that flow and chemical weathering rates have remained essentially constant over the past 10–15 kyr. Estimates of flow in the unsaturated zone using any chemical method may be complicated by long-term changes in precipitation or surface vegetation, seasonal variations in moisture content, and increased fluid residence times in finer-grained units.

By considering a deep vadose zone profile, the effects of seasonal variations in moisture content at the surface are mitigated, thus we are estimating long-term deep vadose zone drainage. The agreement between the NaOAc leachate data, which reflects a time-integrated average of the ($^{234}U/^{238}U$) of pore water recorded by the calcite, is similar to the measured pore water values, suggesting that infiltration and dissolution rates have remained fairly constant over time. If a finite difference approach is used to model Eq. (8), the effect of variable fluid residence times in the fine and coarse-grained units will be accounted for explicitly in the model.

The last term in Eq. (8), which describes the adsorbed uranium, has a small effect on the activity ratio of the pore fluid (or the calculated value of Sk_f) if the retardation factor (K_r) is less than approximately 100. The adsorption of U is highly dependent on the speciation of the aqueous solution. Under oxidizing conditions in the presence of carbonate, the uranium is relatively mobile as anionic carbonate complexes ($UO_2(CO_3)_2^{2-}$, etc.) (Gascoyne, 1992; Gamerdinger et al., 2001). Over the range of pH values observed in the Hanford sediments (pH ~ 7–8), these uranyl carbonate complexes dominate the aqueous speciation, and the adsorption of U is significantly decreased. Values for the U distribution coefficient, K_d, measured at the Hanford Site range from 0.06 to 4 mL/g for natural groundwater conditions (Gamerdinger et al., 1998). For K_d values of 0.6 mL/g, the proposed value for uncontaminated vadose zone sediments (Kincaid et al., 1998), the retardation factor (K_r) would be approximately 1.2–4.0, depending on the water content, therefore the effect of adsorption is much less important than the dissolution, α-recoil, and transport terms.

5.2. The α-recoil length of ^{234}Th in natural minerals

α-Recoil length is a critical parameter for U-series models, but the value is poorly known. α-Recoil lengths have been estimated using a number of different observational techniques. The majority of range estimates for ^{234}Th in natural minerals comes from observations of α-recoil etch pits developed along the cleavage surfaces of minerals, typically micas (Table 7). These studies suggest values between 20 nm for albite (Turkowsky, 1969) and 30 nm for mica group minerals (Huang and Walker, 1967; Coleman et al., 1993; Gogen and Wagnerm, 2000). The results from etch pit studies have been questioned because (i) the leaching procedure used to reveal the tracks also removes some fraction of the original track (Brown and Liu, 1996; Fleischer, 2003), (ii) the leaching process may have enlarged the tracks (Coleman et al., 1993), or (iii), as the particle loses energy, the ionization density increases with distance traveled, thus observations of α-recoil tracks may not account for the total distance traveled by the recoiling nucleus because early portions of the track are not visible (Fleischer, 2003).

Table 7
Summary of measurements for the α-recoil range of ^{234}Th in natural minerals, and theoretical calculations using the binary collision approximation SRIM (Ziegler, 1996)

Mineral	Density	Observed range (nm)	Theoretical range (nm)	Straggling (nm)
UO_2	11.0	12[a]	13.7	7.3
U_3O_8	8.5	19[a]	17.1	8.7
Zircon	4.5	55[b]	22.7	7.2
Muscovite	2.8	20–50[c]	28.4[d] (29.5[e])	5
Feldspar (albite)	2.7	20[f]	30.0	5.8
Calcite	2.7	nd	29.8	5.9
Kaolinite	2.6	nd	30.0	5.4
Gibbsite	2.3	nd	36.9	8.4

nd, not determined.
[a] Hashimoto et al. (1981).
[b] Measurement of ^{234}Th enrichment from zircon (Kigoshi, 1971) interpreted with Eqs. (9a)–(9c).
[c] Etching of α-recoil tracks in muscovite with RF plasma (Gogen and Wagnerm, 2000).
[d] $KAl_3Si_3O_{10}(OH)_{1.8}F_{0.2}$.
[e] Theoretical value for phlogopite from Jonckheere and Gogen (2001).
[f] Observation of artificially produced alpha-recoil tracks via chemical etching (Turkowsky, 1969).

The only study to measure α-recoil loss directly from a solid is that of Kigoshi (1971), from which a range of 55 nm for ^{234}Th in zircon sand was derived. This range value is probably too high because Kigoshi (1971) used a simple geometric model to estimate the surface area of the zircon, and spherical geometric surface areas are commonly a factor of 2–10 less than measured surface areas (Anbeek, 1993; Hochella and Banfield, 1995).

The range for any ion can also be calculated using a binary collision approach (Ziegler et al., 1996). Table 7 summarizes the existing literature values, and those expected from theoretical calculations using the computer model SRIM (Ziegler et al., 1996; Jonckheere and Gogen, 2001). For the reasons discussed above there is considerable variation between the measured and the theoretical values, although the mineral density is still the predominant influence on the calculated α-recoil lengths. Based on theoretical calculations, the α-recoil lengths for natural minerals are expected to increase in the order: zircon < phlogopite < plagioclase ⩽ calcite ⩽ kaolinite < gibbsite (Table 7). The theoretical value of 30 nm for feldspar is used here in calculation of the α-recoil loss parameters.

5.3. Approaches to estimating the α-recoil loss fraction

5.3.1. Geometric considerations

Kigoshi (1971) first proposed that estimates of the α-recoil loss fraction, f_α, can be made according to a simple geometric formulation based on the ratio of surface area to volume for a spherical grain:

$$f_\alpha = \frac{3\lambda_r}{2}\left(\frac{L}{d_p}\right) - \frac{1}{2}\left(\frac{L}{d_p}\right)^3, \quad (9a)$$

where L is the range of recoil ^{234}Th (~20–50 nm in silicates), d_p is the diameter of the particle and λ_r is a correction for surface roughness. For $L \ll d_p$, this expression simplifies to

$$f_\alpha = \frac{3\lambda_r L}{2d_p}. \quad (9b)$$

The equation can be amended for other grain geometries (Fig. 6). For example, for a circular plate with diameter d_p and thickness d_p/n, the equivalent to Eq. (9b) is

$$f_\alpha = \frac{3\lambda_r n L}{2d_p}. \quad (9c)$$

Both Eqs. (9b) and (9c) are statements of the surface-to-volume ratio. If the specific surface area (S) of a material can be measured, then it should be possible to translate that measurement to an estimate of f_α, as long as $d_p \gg L$:

$$f_\alpha = \frac{1}{4} L \cdot S \cdot \lambda_r n \cdot \rho_s. \quad (10)$$

It is typical that measured surface areas are larger than those that come from simple geometrical models (cf. Table 1). A widely used method for measuring sediment specific surface area is the BET (Brunauer–Emmett–Teller) gas adsorption method. The conversion of BET measurements to estimates of f_α may not be straightforward. Gas adsorption surface area measurements (BET) reflect the available surface area for small gas molecules (N_2 or Kr) with a diameter of ~0.3 nm, which is about 100 times smaller than the recoil distance. Consequently, nm-scale surface roughness can add to the BET surface area but may not significantly affect f_α. It is expected, therefore, that the BET method will overestimate the surface area applicable to estimating α-recoil effects, and possibly reactive surface area in general. The BET surface areas we measured on fresh sediment are much larger than geometric predictions based on the grain size distribution, and thus correspond to f_α values that are about 10–20 times larger. We conclude therefore, that the BET surface areas are strongly affected by nanoscale surface roughness that does not affect α-recoil loss.

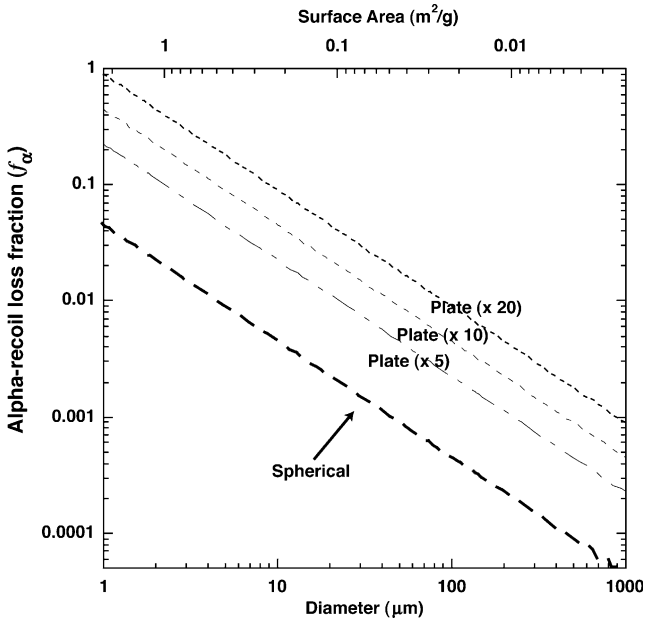

Fig. 6. Comparison of physically based models for α-recoil loss fraction. Dark stippled line corresponds to the spherical model, light stippled contours lines correspond to model for plate geometry with different values of d_p/n (5, 10 and 20), [see Eq. (9c) in text].

However, in circumstances where f_α is constrained by isotopic measurements, it may be possible to estimate the surface area of the material in intimate contact with the fluid (Maher et al., 2006). This technique may be especially useful in porous media, where the reactive surface area is difficult to measure.

5.3.2. Geometric estimates of the α-recoil loss fraction in natural sediment

For soils or sediment with variable grain size, the estimate of α-recoil loss must incorporate the fact that the different grain size fractions contribute to the bulk value of f_α according to surface area rather than volume- or weight fraction. If the grain size distribution is known, then the f_α factor can be calculated by summing the contributions from each grain size fraction:

$$F_\alpha = \sum_n \lambda_r n X_{\overline{d_p}} f_\alpha(\overline{d_p}), \quad (11)$$

where F_α is the weighted value for the bulk sediment, X_{d_p} is the mass or volume fraction of sediment in the grain size interval n, and d_p is the mean particle diameter for the grain size interval n. The effect of grain size distribution on F_α is illustrated in Fig. 7, where F_α is plotted as a function of mean grain size and standard deviation of the natural logarithm of the grain size (σ) for sediment with a lognormal grain size distribution. For sediment with the same mean grain size, the sediment with a larger standard deviation will have a higher F_α value because of the greater loss of ^{234}Th from the fine-grained fractions. Fig. 7 shows that knowledge of the mean grain size is insufficient to accurately estimate F_α from geometrical models. For example, at 12 m depth the mean grain size is 100 μm corresponding to an f_α of 0.0004. In contrast, the value predicted by Eq. (11) is 0.007, a factor of ~20 greater due to the substantial contribution of the fine-grained material. The grain size distributions reported in Serne et al. (2002) were used to estimate a weighted geometric α-recoil loss factor (F_α). The median diameter and weight fraction for each grain size interval was used to calculate f_α using the spherical model (Table 8). These calculations assume a surface roughness factor of 1, an assumption that will be explored further in the following section.

5.3.3. Measured depletion in fine-grained sediments

For the primary silicate mineral, the ^{234}U concentration in the dissolving solid is given by

$$\frac{\partial C_{s,234}}{\partial t} = \lambda_{238} C_{s,238} - f_\alpha(S, d_p)\lambda_{238} C_{s,238} - \lambda_{234} C_{s,234}, \quad (12)$$

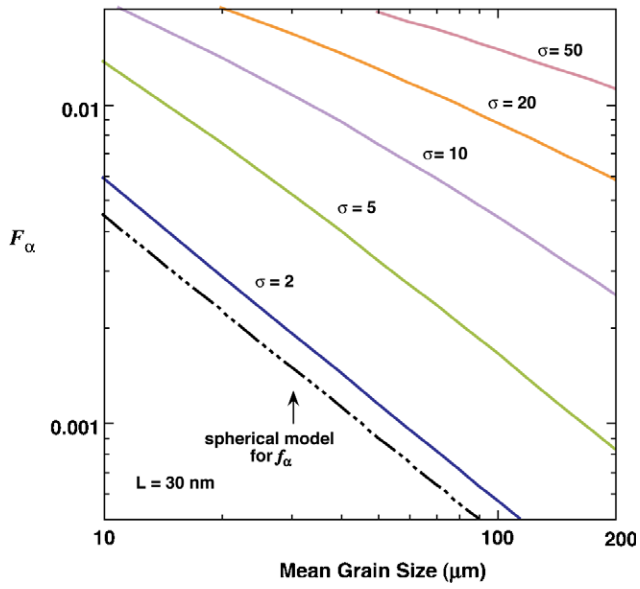

Fig. 7. Weighted α-recoil loss factor for lognormal grain size distribution and standard deviation (σ). In heterogeneous sediments, the α-recoil loss factor cannot be predicted by only the mean grain size.

Table 8
f_α values for the <45 μm size fraction calculated from measurement of the solids and from the grain size distribution using the geometric models

Depth (m)	f_α <45 μm ($1 - A_s$)	Geometric model		
		% <45 μm	F_α <45 μm (grain size)	% of total F_α
HFSD1				
0.3	0.033			
1.8	0.036			
2.9	0.036			
6.0	0.053			
8.8	0.053			
12.0	0.012	22.3	0.007	95.5
HFGD				
14.5		16.7	0.007	99.3
17.6	0.015			
HFSD2				
21.0	0.017			
26.4	0.009			
27.9		37.8	0.010	98.6
30.9		21.3	0.007	96.0
32.3	0.007[a]			
37.9	0.028[a]			
CCUf				
41.5		81.5	0.024	99.3
CCUc: 44.5		30.6	0.006	99.3
Rtf				
45.1		13.8	0.010	98.9
46.2	0.039			
49.8	0.024	11.0	0.006	96.0

[a] From NaOAc pre-treated samples.

where f_α is a function of the grain radius (d_p) and the surface area (S). The corresponding equation for the activity ratio is given by

$$\frac{\partial A_s}{\partial t} = A_s(\lambda_{238} - \lambda_{234}) + \lambda_{234}[1 - f_\alpha(S, d_p)]. \quad (13)$$

At steady state, the activity ratio of the solid is equal to $1 - f_\alpha$, assuming that $\lambda_{238} - \lambda_{234} = -\lambda_{234}$. For sediments that are less than about 1 Ma, the solids may not be in steady state, and hence $(1 - f_\alpha) \leqslant A_s$. For sediments of an appropriate age, an estimate of f_α can be made based on the measured ($^{234}U/^{238}U$) ratio of the solid if an appropriate grain size is selected. For the 299-W22-48 sediments, the median grain size varies from 40 μm in the CCUc Unit to 1 mm in the Hanford Formation. For grain sizes larger than about 100 μm, the expected value of f_α is too small to be measured accurately as $1 - A_s$. However, because there is a substantial amount of fine-grained material in all of the samples (between 20% and 5% of the total sediment is in the <45 μm fraction), 90–100% of the total recoil loss of ^{234}U is from the <45 μm fraction. Thus, the ($^{234}U^{238}U$) values of the <45 μm fraction should provide a direct measure f_α.

In Fig. 8, the bulk sediment f_α values calculated from measurements of the <45 μm fraction (Table 5b and Fig. 5), are compared with estimates based on the weighted

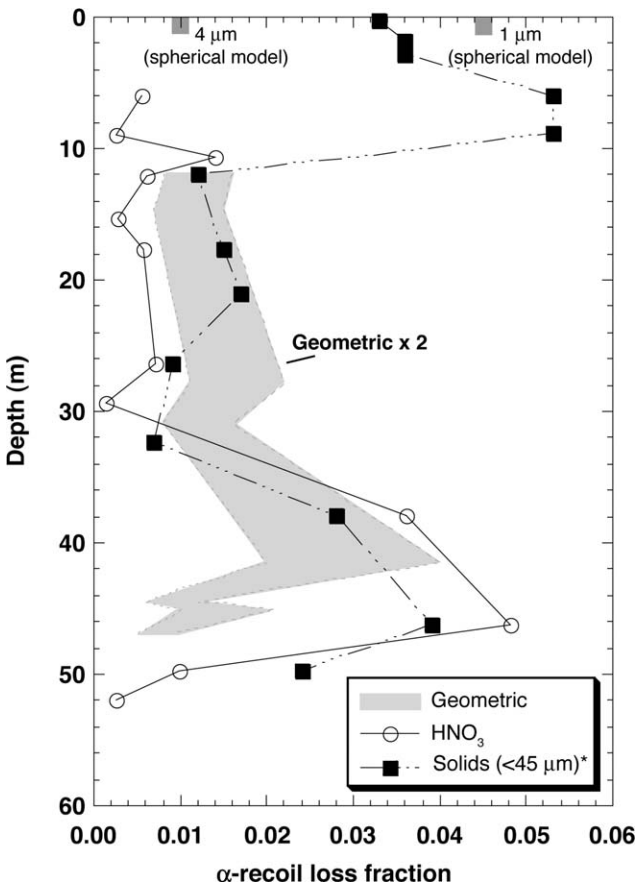

Fig. 8. Comparison of estimates for the α-recoil loss factors. A summary of the model formulations is given in Table 9. The shaded region for the geometric model corresponds to the range for surface roughness values between 0 and 2. The size fraction values are calculated using the values from the samples that were not pretreated, except where noted in Table 8.

geometric α-recoil loss factor (F_α) for the <45 μm fraction (Eq. (11)). The α-recoil loss factors calculated from the ($^{234}U/^{238}U$) measurements of the untreated <45 μm fraction agree well with the geometric estimate provided by Eqs. (9a) and (11). The agreement suggests that the geometric estimate assuming spherical grains may be reasonably accurate as long as the grain size distribution of the sediment is taken into account. In addition, a comparison of these two techniques suggests that the surface roughness applicable to these sediments is approximately 2 (Fig. 8).

5.3.4. Measured depletion in mineral surfaces

Strong nitric acid leaches of the bulk Hanford sediments show significant depletions in the ($^{234}U/^{238}U$) ratios (Table 4). These leaches may reflect dissolution of the surface layers of the individual grains and therefore provide an independent measure of f_α. If it is assumed that the remaining (unleached) U in the sediment has ($^{234}U/^{238}U$) = 1, the nitric acid leach data can be converted to f_α by

$$f_\alpha = (1 - A_L)\frac{[U]_L}{[U]_{solid}}, \tag{14}$$

where A_L is the activity of the strong leach assumed to represent the material undergoing dissolution, and $[U]_L/[U]_T$ is the fraction of U leached. The estimates of f_α derived from Eq. (14) are shown in Fig. 8. The f_α estimates derived from the nitric acid leach data are slightly different from those obtained from the other approaches, but are in the same general range of 0.004–0.03. Further experimentation is necessary to determine the optimal leach procedure for calculating the α-recoil loss fraction by this technique.

5.3.5. Surface depletion and non-steady state α-recoil loss

For simple grain geometry such as a smooth sphere, the depletion of ^{234}U should be a maximum at the grain surface and should decrease to zero over a distance L from the grain surface toward the grain center. The radial concentration of ^{234}U in the solid can be described by

$$\frac{\partial C_{234}(r)}{\partial t} = -\lambda_{234}C_{234} + \lambda_{238}C_{238}\varphi(r), \tag{15}$$

where λ is the decay constant, C_i is the concentration, and $\varphi(r)$ is a geometric distortion function that describes the loss of ^{234}U as a function of the radial distance. For a spherical object $\varphi(r)$ is equal to (Ribeiro, 1998; and references within):

$$\varphi(r) = \frac{1}{2} + \frac{a^2 - L^2}{4Lr} - \frac{r}{4L} \tag{16}$$

with the radius equal to a, and r is the radial distance. Eq. (16) applies to the interval $a - L < r < a$ for $r < a - L$, $\varphi(r) = 1$. The ($^{234}U/^{238}U$) ratio as a function of time is

$$\frac{\partial A_s}{\partial t} = -\lambda_{234}A_s + \lambda_{234}\varphi(r) + \lambda_{238}A_s. \tag{17}$$

The cross-sectional depletion for a grain at steady state is shown in Fig. 9. Eq. (17) can be solved to yield the activity ratio as a function of time and radial distance:

$$A_s[t, r] = A_{s,0}e^{(-\lambda_{234})t} + \varphi(r)[1 - \exp^{-\lambda_{234}t}]. \tag{18}$$

Fig. 9 also shows the evolution of the surface layer of the grain with time under the assumption that the grain starts (at $t = 0$) with the secular equilibrium value of $A_s = 1$. The ^{234}U depletion in the surface layer increases progressively with time until it reaches the steady state value at about 1 million years. For "freshly eroded" sediments, the activity ratio is not the steady state value, and therefore the activity ratio of the bulk solid will not fully reflect the α-recoil loss factor ($f_\alpha > 1 - A_s$). Also, the depletion of the grain surface should affect the ($^{234}U/^{238}U$) of the U flux to the pore water via dissolution.

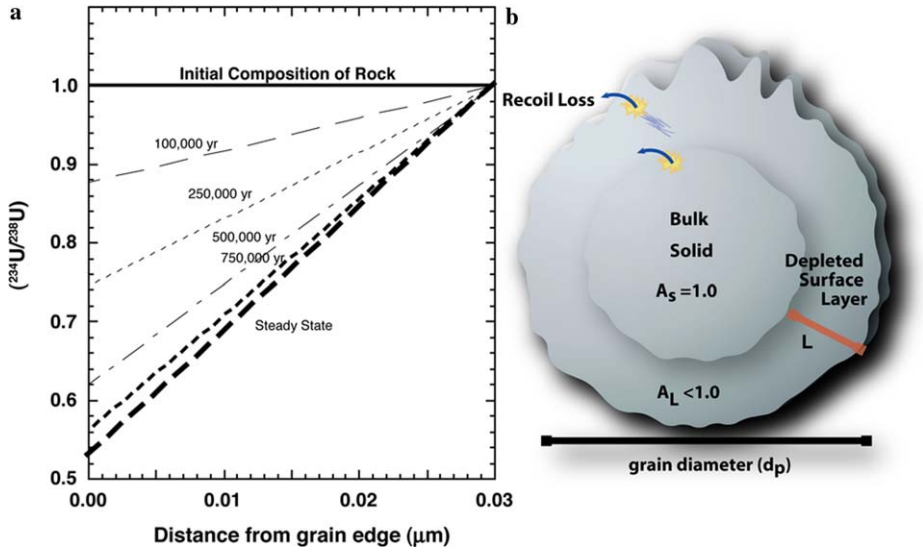

Fig. 9. Evolution of the surface layer activity ratio. (a) Predicted α-recoil loss along the cross-section of the surface of a spherical grain as a function of time. (b) Schematic of grain subject to α-recoil loss showing depleted surface layer.

5.3.6. Preferential leaching

Leaching from radiation damaged sites and implantation could provide an additional contribution to ^{234}U-loss not accounted for by α-recoil. The oxidation of the $^{238}U^{4+}$ nuclide to $^{234}U^{6+}$, and damage to the crystal lattice during the α-decay process may result in some preferential dissolution of ^{234}U. The relationship between these damaged regions and the surface morphologies observed in weathered grains is unknown, and quantifying these effects at the microscopic scale is nearly impossible because of the relatively low concentrations of U in natural materials and the long half-life of ^{238}U. In addition, very few studies have measured the depletion in the solids, or carefully considered the effect of different grain sizes.

The α-recoil loss fraction calculated from the measured depletion in the ($^{234}U/^{238}U$) of the <45 μm fraction, when compared to the geometric estimate based on the grain size distribution, suggests that all of the measured solid depletion can be accounted for by careful consideration of the α-recoil processes. If leaching were an important factor in these sediments, we would expect to see the much higher f_α values and greater depletion in the ($^{234}U/^{238}U$) of the <45 μm fraction relative to the geometric estimate. The data presented here and for deep-sea silicate sediments (Maher et al., 2004, 2006; DePaolo et al., 2006) suggests that the effect of leaching in slowly dissolving silicate sediments is trivial compared to the α-recoil loss from the solids.

5.4. Summary of α-recoil loss rate estimates for Hanford sediments

Table 9 presents a summary of the methods used to calculate the α-recoil loss fractions for the Hanford sediment shown in Fig. 8. The chemical approaches using the nitric acid leach data or the <45 μm fraction predicts f_α values that are similar to those predicted by the geometric model. All three models also show similar trends as a function of depth. The BET surface areas are much larger than those calculated with the geometric model, and correspond to f_α values that are about 10–20 times greater than the nitric acid leach values, the measured depletion in the <45 μm fraction, or the grain size estimates. We conclude therefore, that the BET surface areas are strongly affected by nanoscale surface roughness that does not affect α-recoil loss.

Errors in our f_α values come from several factors. For the grain size distributions, the median value for each grain size interval was taken, whereas the α-recoil loss factor is not linear within an interval; therefore the estimates may be slightly low. For the nitric acid leach procedure, a small fraction of the U is derived from secondary precipitates ($CaCO_3$) with relatively high ($^{234}U/^{238}U$) therefore the measured activity ratios may be too high by 1–2%. The distribution of U within the mineral assemblage is also an issue. We assume that the majority of the uranium is contained in the feldspars at an average concentration of 1.0-2.0 ppm. Minerals with higher U concentrations (such as zircon, monazite, U minerals, etc.) would have substantially greater mineral-specific α-recoil loss rates, but because such minerals are generally present in trace quantities they have a small effect on the overall rate. For example, normative calculations for the Hanford sediments suggest 0.03 wt% zircon on average. Assuming zircon with 300 ppm U (an average value for crustal zircons) at 0.03 wt%, and plagioclase at 50 wt% and 2 ppm U, the overall plagioclase rate is approximately 10 times greater than for zircon (assuming the same f_α values). For the present purposes we assume that these minerals have a negligible effect on the overall α-recoil loss budget because they make up a fairly small percentage of the total sediment. However, as these calculations illustrate, further work should be done to quantify the importance of trace mineral phases on $^{234}U/^{238}U$ disequilibrium.

5.5. Estimates of the infiltration and weathering rate for Hanford sediments

5.5.1. Previous estimates of infiltration and dissolution from pore water $^{87}Sr/^{86}Sr$

Sr isotopes in pore water and sediment in 299-W22-48 were interpreted previously in Maher et al. (2003). The

Table 9
Summary of α-recoil loss models

Model	Equation for f_α	Method
Spherical grain	$f_\alpha = \frac{3}{2}\left(\frac{L}{d_p}\right) - \frac{1}{2}\left(\frac{L}{d_p}\right)^3$	This model applies to material with uniform grain size, and assumes the geometry is well represented by a sphere (cf. Eqs. (9b) and (9c), Kigoshi, 1971)
Weighted geometric	$F_\alpha = \sum_n X_{\overline{d_p}} f_\alpha(\overline{d_p})$	The f_α value is calculated for the median diameter within each grain size interval, then weighted according the weight fraction of each grain size interval
Surface area	$f_\alpha = \frac{1}{4} L \cdot S \cdot \rho_s$	If the geometric surface area is known, the f_α value can be calculated. Our data suggest that BET-type measurements of surface area may over predict the α-recoil loss. Conversely, the surface area of the material could be extracted if the α-recoil loss fraction is known
Size fraction	$f_\alpha = 1 - A_s$	This model assumes the ($^{234}U/^{238}U$) values are at steady state, and that the depletion in the solids can be measured. Applicable to fine-grained material approximately 5–45 μm in diameter and older than approximately 500 ka (cf. Christensen et al., 2004; DePaolo et al., 2006)
Strong acid leach	$f_\alpha = (1 - A_L)\frac{[U]_L}{[U]_{solid}}$	The strong acid leach ($^{234}U/^{238}U$) values are weighted according the fraction of U leached. This assumes that the material dissolved by the leach reflects the depleted surface of the minerals

pore water $^{87}Sr/^{86}Sr$ at the top of the profile are quite high (0.721) and decrease towards the isotopic ratio of the bulk sediment (0.711) with depth. This effect is interpreted as a balance between dissolution of the sediment, which contributes low-$^{87}Sr/^{86}Sr$ to the pore water, and downward infiltration. The high $^{87}Sr/^{86}Sr$ of the pore water in the upper 5 m is most likely the result of rapid preferential weathering of a mineral with higher $^{87}Sr/^{86}Sr$ ratios, such as biotite.

A steady state finite difference model of the pore fluid $^{87}Sr/^{86}Sr$ (r_f) was used to extract the ratio of the dissolution rate to the infiltration flux (Sk_d/q) using an isotopic reactive-transport formulation (Maher et al., 2003):

$$\frac{\partial r_f}{\partial z} = \frac{\theta M_s S k_d C_s}{q C_f}(r_s - r_f) \tag{19}$$

similar to that of Eq. (8) given previously for pore fluid ($^{234}U/^{238}U$).

Estimates of feldspar dissolution rates in soils of similar age and mineralogy from White et al. (1996) were used to constrain the infiltration flux to 7 ± 3 mm/yr. The Sr isotope data and corresponding model profiles for the ratio of (Sk_d/q) are shown in Fig. 10. The inferred dissolution rate from the Sr isotopes increases as a function of increasing infiltration rates, thus the pore water $^{87}Sr/^{86}Sr$ responds oppositely to the effect of infiltration compared to the pore water ($^{234}U/^{238}U$). As implied by the uranium data shown in Fig. 3, infiltration and dissolution decrease the pore water ($^{234}U/^{238}U$) values. Thus, as the infiltration rate increases, the inferred dissolution rate must decrease in order to maintain the measured ($^{234}U/^{238}U$) in the pore water. The contrasting behavior of these two isotopic systems suggests that it may be possible to combine them to create a coupled isotopic model that will yield unique values for both the infiltration and dissolution rates.

5.5.2. Coupled U–Sr model for dissolution/infiltration

The ($^{234}U/^{238}U$) values in the pore waters of the Hanford Formation increase steadily with depth over the upper 45 m, until the contact with the calcic paleosol unit where the activity ratios decrease dramatically to approximately 1.05. The values in the Ringold pore waters (>50 m depth) lie along the extrapolation of the near-linear trend of the upper profiles. In order to generate the low pore water ($^{234}U/^{238}U$) values observed in the calcic paleosol unit, silicate weathering rates would have to increase dramatically, then decrease rapidly subsequent to the calcic paleosol, within the Ringold Formation. Evidence for rapid weathering was not observed in the Sr isotopic profiles. In addition, the ($^{234}U/^{238}U$) values of the nitric acid leach, which presumably dissolved the majority of the carbonate, were also much higher than the pore water (1.09). Given that rapid weathering does not appear likely and the consistent trend observed in the surrounding pore waters, we infer that the pore water of the calcic paleosol has most likely been influenced by lateral flow of water from previous site activities. Evidence for lateral migration of water into the 299-W22-48 borehole at this depth was also observed in the $\delta^{18}O$ of the pore water (DePaolo et al., 2004); and elevated amounts of NO_3, Cr, and ^{99}Tc were also detected at this depth (Serne et al., 2002). In the analysis of the 299-W22-48 borehole, we assume that prior to the recent perturbation, the pore water values of the Cold Creek unit were closer to the general trend of the remainder of the data,

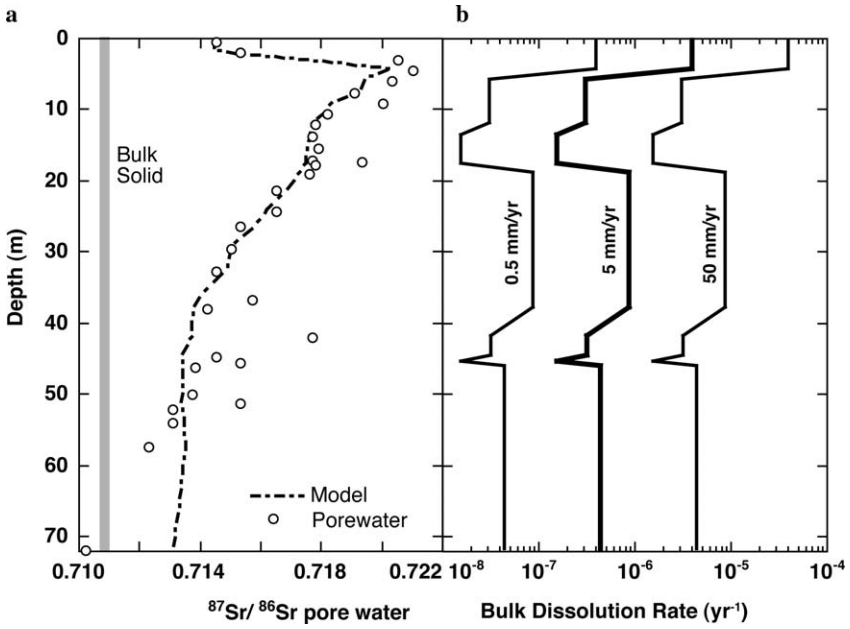

Fig. 10. (a) $^{87}Sr/^{86}Sr$ and model dissolution rates as a function of different assumptions for infiltration flux modified from Maher et al. (2003). The pore water data was modeled using the finite difference Eq. (19) to extract the ratio of dissolution rate to the infiltration flux (R_d/q). (b) As the inferred infiltration rate increases in the model, the bulk dissolution rate must also increase in order to maintain the same fit to the pore water data.

and any calculated values for this unit are treated as highly uncertain. The (^{234}U/^{238}U) of NaOAc leachate data at the Hanford Site is in general reflective of the present day pore water values suggesting that major perturbations to the hydrology have not occurred in the last 15,000 years.

The pore water activity ratio as a function of depth can be approximated by

$$\frac{\partial A_f}{\partial z} = \frac{\theta M k_{f,i} S C_s}{q C_f}(A_s - A_f) + \frac{\lambda_{234}}{q}\left(\frac{\theta M_s f_\alpha C_s}{C_f}\right). \quad (20)$$

This equation predicts that as infiltration rates increase in the system, the pore water (^{234}U/^{238}U) values will shift towards the value of the dissolving solid, and for low infiltration rates the pore water values should increase. A steady state finite difference approach is used to evaluate the reaction rates and infiltration flux consistent with the (^{234}U/^{238}U) pore water data. The (^{234}U/^{238}U) values from the nitric acid leaches are used to represent the activity of the dissolving solid. The f_α values used are the estimates based on the (^{234}U/^{238}U) of the <45 μm fraction, although all three approaches were evaluated.

Assuming that the ratio of the dissolution rate to the infiltration flux (Sk_f/q) determined from the Sr isotope model applies to the (^{234}U/^{238}U) system, the infiltration and reaction rates consistent with the measured (^{234}U/^{238}U) and ^{87}Sr/^{86}Sr of the pore water can be determined. The best fit to the data is for an infiltration rate of 5 ± 2 mm/yr (Fig. 11). In the upper 5 m and again in the region from about 20 to 40 m, slower reaction rates were required to fit the U data (Fig. 11b). The elevated dissolution rates in the upper 5 m of the Sr model were previously interpreted to reflect preferential weathering of a radiogenic mineral such as biotite—this effect may also be present in the lower portions of the profile. The U model is less likely to be influenced by trace mineral phases as reflected by the relatively constant dissolution rates. Although certain minerals such as zircon and apatite may have high U concentrations, they are quite insoluble and will not have (^{234}U/^{238}U) values substantially different than the bulk sediment. The general agreement between the dissolution rate profiles suggests that the isotopic approach is a useful monitor of the bulk dissolution rates.

These calculated rates reflect a long-term (ca. 10–15 ka) average of flow and chemical weathering, and are valid only for diffuse meteoric recharge. Flow and dissolution in the unsaturated zone may be considerably more complicated than represented here, however the data require both infiltration and dissolution within the profile. For instance, if the weathering rate is zero, the uranium profile is consistent with the data at a higher infiltration rate (~10 mm/yr), and the pore water (^{234}U/^{238}U) becomes a function of only the α-recoil loss factor and the infiltration flux. However, this scenario would not be consistent with the Sr model, as the Sr-derived infiltration flux would be zero. If the infiltration flux is very low, then the weathering rates required to fit the isotopic data would diverge, as the weathering rate computed from the Sr isotopes increase as a function of increasing infiltration, and conversely for the U isotopes.

Each of three models for calculating f_α were also evaluated. None resulted in substantial changes to the estimated

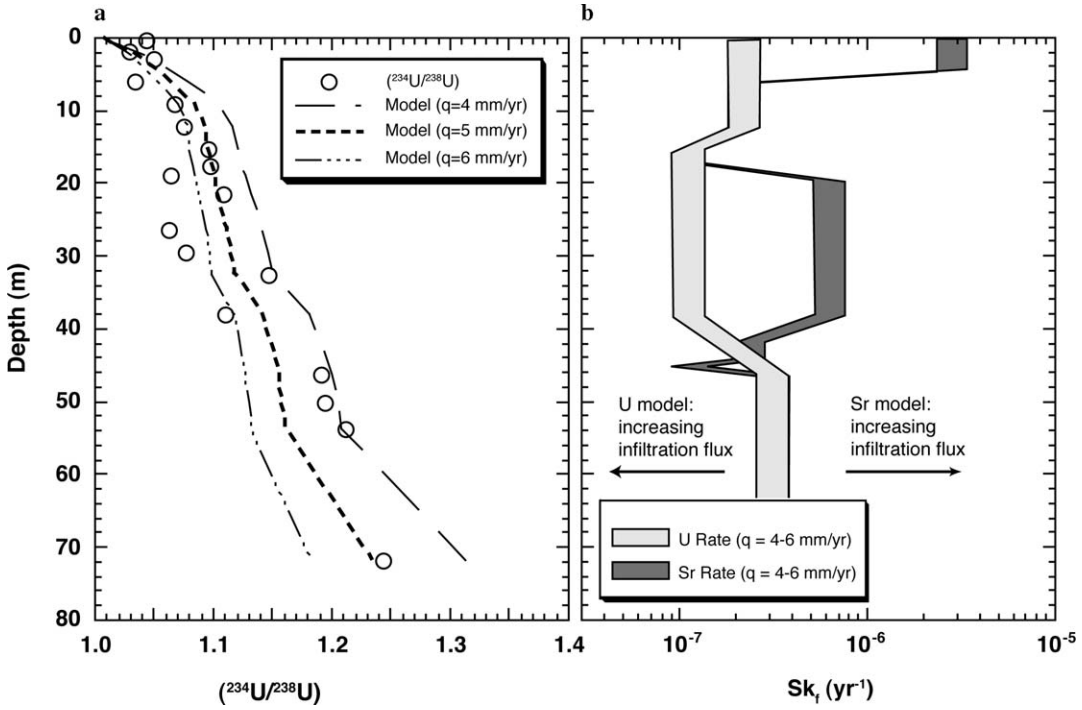

Fig. 11. (a) Model for pore water (^{234}U/^{238}U). (b) Model for U infiltration flux and reaction rate compared to rates from Sr isotopes. The two models are consistent with infiltration rate of 5 ± 2 mm/yr, the lower bound of the range predicted from the Sr model based on an independent estimate of the dissolution rates.

Table 10
Weathering rate constants for Hanford sediments calculated using the geometric surface area and a formula weight for plagioclase of 270 g/mol

Formation	Estimated age (Ma)[a]	Surface area (m^2/g)[b]	log k_f ($mol/m^2/s$)
HFSD1 (12.5 m)	0.015	0.39	-15.75 ± 0.4
HFGD (12.5–18.6)	0.015–0.78	0.36	-16.46 ± 0.4
HFSD (18.6–41.2)	1.77–1.95	0.56–0.41	-16.31 ± 0.4
Rtf (44.5–71.8)	>3.4	0.34	-16.29 ± 0.4

[a] Based on paleomagnetic data and other evidence from Bjornstad et al. (2001).
[b] From geometric estimate.

infiltration flux. The nitric acid leach values, which are slightly lower than the geometric and size fraction estimates, require infiltration fluxes of 2 mm/yr, while the geometric estimate with $\lambda_r = 2$ resulted in no change. If the f_α values are much greater (i.e. there were additional α-recoil sources that are not accounted for in our estimates), then both the infiltration rate and the dissolution rate must increase proportionally in the model. Lastly, variations in the ($^{234}U/^{238}U$) of the dissolving solid between 0.5 and 1.0 resulted in values for q of 3 and 6 mm/yr and for $A_s = 0.5$ and 1.0, respectively.

Given the above constraints, we suggest that the infiltration flux is around 5 ± 2 mm/yr. This range is only slightly lower than the value reported previously (7 ± 3 mm/yr) in Maher et al. (2003). These infiltration rates agree with recent estimates using other approaches. Based on stable isotopes in pore water from this borehole, DePaolo et al. (2004) estimated values of ca. 10 mm/yr. Numerical modeling results for the 200 Area suggest infiltration fluxes of $\lesssim 1$ mm/yr (Singleton et al., 2006) to 3 mm/yr (Fayer and Walters, 1995), compared to a site-wide estimate of between 1.2 and 12.7 mm/yr (Bauer and Vaccaro, 1990) (see also Table 6, Maher et al., 2003). Chloride mass balance estimates from near the 200 Area suggest values that are substantially lower, from 0.1 to 0.01 mm/yr (Murphy et al., 1996). This discrepancy may be due to differences in the hydrology or, more likely, the last flood at the Hanford Site (ca. 10–15 ka) may not have flushed all of the previously accumulated chloride from the system.

The original dissolution rates used to constrain the infiltration flux for the Sr model were derived from values for granitic chronosequences reported by White et al. (1996). The dissolution rates determined here are lower than these values by only a factor of approximately 1.4. When converted to the traditional units of a dissolution rate constant, the values calculated for the Hanford sediments are $10^{-15.75}$ to $10^{-16.5}$ $mol/m^2/s$ (Table 10). These values are consistent with the values reported from other natural systems of a similar age (cf. White and Brantley, 2003).

6. Conclusions

The α-recoil loss factor, f_α, is an integral component of U-series applications. Because the f_α parameter influences the rate of increase of the ($^{234}U/^{238}U$) values, subtle variations in the α-recoil loss fraction (possibly combined with variations in the activity of the dissolving solid), can substantially affect inferences about the weathering rate and fluid flow. A comparison of different methods for capturing the α-recoil loss parameter suggests that either geometric or bulk dissolution techniques that carefully consider the grain size distribution of the sediment, or chemical leach procedures that remove some fraction of the depleted surfaces of the sediment, provide a means of quantifying the α-recoil loss in heterogeneous natural sediments. The later may be preferred in fractured systems where grain size estimates would not be available.

The coupled application of U and Sr isotopes, which are both sensitive indicators of fluid–rock interaction, offers a means of estimating infiltration fluxes and dissolution rates *in situ* without invasive instrumentation or the typical age constraints required for weathering studies (i.e. chronosequences or long term soil monitoring). The reaction rates inferred from these models respond oppositely to the effect of fluid flow—calculated Sr reaction rates will in general increase with increasing infiltration rates because the $^{87}Sr/^{86}Sr$ of the pore fluid changes as a function of Sk_f/q and the difference between the isotopic ratios of the dissolving solid and the fluid. In contrast, the ($^{234}U/^{238}U$) of the pore fluid responds as a function of $(f_\alpha - k_f)/q$, thus if q increases, the inferred weathering rate would be slower. This provides two independent estimates for two generally unknown parameters. The opposing behavior of these two isotopic systems suggests that their integration into more powerful numerical reactive transport formulations would make them a useful tool in studies of reactive flow. The application of these two isotopic systems is probably best assessed by the use of more powerful numerical tools than those employed here, such as reactive transport formulations that include provisions for these isotopic species, and may consider other geochemical parameters such as saturation state of the minerals with respect to the fluids.

Acknowledgments

We acknowledge Tom Owens for his assistance in the laboratory and Evan Dresel and Jeff Serne at PNNL for help in obtaining samples and for providing site information. Reviews of the manuscript by L. Neymark, A. Jacobson and several anonymous reviewers are greatly appreciated. Funding was provided by the Department of Energy under contract DE-AC02-05CH11231 through the Hanford Science and Technology Program, and by the Director, Office of Science, Basic Energy Sciences, Chemical Sciences, Geosciences and Biosciences Division of the U.S. Department of Energy and the Assistant Secretary of the Office of Environmental Management, Office of Science and Technology, Environmental Management Science Program, of the U.S. Department of Energy, both under Contract No. DE-AC03-76SF00098 to LBNL.

Associate editor: S. Krishnaswami

References

Anbeek, C., 1993. The effect of natural weathering on dissolution rates. *Geochim. Cosmochim. Acta* **57** (21–22), 4963–4975.

Bauer, H.H., Vaccaro, J.J., 1990. *Estimates of Ground Water Recharge to the Columbia Plateau Regional Aquifer System; Washington, Oregon and Idaho for predevelopment and Current Land Use Conditions*. U.S. Geological Survey, WRIR 88-4108.

Bjornstad, B.N., Fecht, K.R., Pluhar, C.J., 2001. Long history of pre-Wisconsin, Ice Age cataclysmic floods: evidence from southeastern Washington State. *J. Geol.* **109** (6), 695–713.

Bonotto, D.M., Andrews, J.N., 2000. The transfer of uranium isotopes U-234 and U-238 to the waters interacting with carbonates from Mendip Hills area (England). *Appl. Radiat. Isot.* **52** (4), 965–983.

Brown, N.M.D., Liu, Z.H., 1996. The etching of natural alpha-recoil tracks in mica with an argon RF-plasma discharge and their imaging via atomic force microscopy. *Appl. Surf. Sci.* **93** (2), 89–100.

Cheng, H., Edwards, R.L., Hoff, J., Gallup, C.D., Richards, D.A., Asmerom, Y., 2000. The half-lives of uranium-234 and thorium-230. *Chem. Geol.* **169** (1-2), 17–33.

Christensen, J.N., Dresel, P.E., Conrad, M.E., Maher, K., DePaolo, D.J., 2004. Identifying the sources of subsurface contamination at the Hanford Site in Washington using high-precision uranium isotopic measurements. *Environ. Sci. Technol.* **38** (12), 3330–3337.

Coleman, R.V., Xue, Q., Gong, Y., Price, P.B., 1993. Atomic-force microscope study of etched tracks of low-energy heavy-ions in mica. *Surf. Sci.* **297** (3), 359–370.

DePaolo, D.J., Conrad, M.E., Maher, K., Gee, G.W., 2004. Evaporation effects on oxygen and hydrogen isotopes in deep vadose zone pore fluids at Hanford, Washington: implications for recharge and horizontal fluid movement. *Vadose Zone J.* **3**, 220–232.

DePaolo, D.J., Maher, K., Christensen, J.N., McManus, J., 2006. Sediment transport time measured with U-series isotopes: results from ODP North Atlantic Drift Site 984. *Earth Planet. Sci. Lett.* **248** (1-2), 379–395.

Dickin, A.P., 1995. *Radiogenic Isotope Geology*. Cambridge University Press, Cambridge.

Fayer, M.J., Walters, M.B., 1995. *Estimated Recharge Rates at the Hanford Site*. Pacific Northwest National Laboratory, PNNL-10285.

Fleischer, R.L., 2003. Etching of recoil tracks in solids. *Geochim. Cosmochim. Acta* **67** (24), 4769–4774.

Gamerdinger, A.P., Kaplan, D.I., Resch, C.T., 1998. *Uranium (VI) Sorption and Transport in Unsaturated, Subsurface Hanford Site Sediments—Effect of Moisture Content and Sediment Texture: Final Report for Subtask 2b*. Pacific Northwest National Laboratory, PNNL-11975.

Gamerdinger, A.P., Kaplan, D.I., Wellman, D.M., Serne, R.J., 2001. Two-region flow and decreased sorption of uranium (VI) during transport in Hanford groundwater and unsaturated sands. *Water Resour. Res.* **37** (12), 3155–3162.

Gascoyne, M., 1992. Geochemistry of the actinides and their daughters. In: Ivanovich, M., Harmon, R.S. (Eds.), *Uranium-Series Disequilibrium: Applications to Earth, Marine, and Environmental Sciences*, second ed. Oxford University Press, Oxford, pp. 34–61.

Gogen, K., Wagnerm, G.A., 2000. Alpha-recoil track dating of Quaternary volcanics. *Chem. Geol.* **166** (1-2), 127–137.

Hashimoto, T., Kido, K., Sotobayashi, T., 1981. Ranges of alpha-recoil Th-234 atoms in uranium-oxides. *J. Inorg. Nucl. Chem.* **43** (10), 2233–2238.

Hochella, M.F., Banfield, J.F., 1995. Chemical weathering of silicates in nature: a microscopic perspective with theoretical considerations*Chemical Weathering Rates of Silicate Minerals*, Vol. 31. Mineralogical Society of America, pp. 353–406.

Huang, W.H., Walker, R.M., 1967. Fossil alpha-particle recoil tracks: a new method of age determination. *Science* **155**, 1103–1106.

Jaffey, A.H., Flynn, K.F., Glendenin, L.E., Bentley, W.C., Essling, A.M., 1971. Precision measurements of the half-lives and specific activities of ^{235}U and ^{238}U. *Phys. Rev.* **C4**, 1189–1906.

Johnson, T.M., DePaolo, D.J., 1994. Interpretation of isotopic data in groundwater–rock systems—model development and application to Sr isotope data from Yucca Mountain. *Water Resour. Res.* **30** (5), 1571–1587.

Johnson, T.M., DePaolo, D.J., 1997. Rapid exchange effects on isotope ratios in groundwater systems. 1. Development of a transport-dissolution-exchange model. *Water Resour. Res.* **33** (1), 187–195.

Jonckheere, R., Gogen, K., 2001. A Monte-Carlo calculation of the size distribution of latent alpha-recoil tracks. *Nucl. Instrum. Methods Phys. Res. Sect. B-Beam Interact. Mater. Atoms* **183** (3–4), 347–357.

Kigoshi, K., 1971. Alpha-recoil thorium-234—dissolution into water and uranium-234/uranium-238 disequilibrium in nature. *Science* **173** (3991), 47–49.

Kincaid, C.T., Bergeron, M.P., Cole, C.R., Freshley, M.D., Hassig, N.L., Johnson, V.G., Kaplan, D.I., Serne, R.J., Streile, G.P., Strenge, D.L., Thorne, P.D., Vail, L.W., Whyatt, G.A., Wurstner, S.K., 1998. *Composite analysis for low-level waste disposal in the 200 Areas Plateau of the Hanford Site*. Pacific Northwest National Laboratory, PNNL-11800.

Krane, K., 1988. *Introductory Nuclear Physics*. Wiley, New York.

Krishnaswami, S., Graustein, W.C., Turekian, K.K., Dowd, J.F., 1982. Radium, thorium and radioactive lead isotopes in groundwaters—application to the in situ determination of adsorption–desorption rate constants and retardation factors. *Water Resour. Res.* **18** (6), 1663–1675.

Ku, T.-L., Luo, S.D., Leslie, B.W., Hammond, D.E., 1992. Decay-series disequilibria applied to the study of rock–water interaction and geothermal systems. In: Ivanovich, M., Harmon, R.S. (Eds.), *Uranium-Series Disequilibrium: Applications to Earth, Marine, and Environmental Science*. Clarendon Press, Oxford, pp. 630–671.

Lindsey, K.A., Slate, J.L., Jaeger, G.K., Swett, K.J., Mercer, R.B., 1994. *Geologic Setting of the Low-level Burial Grounds*. Westinghouse Hanford Company, Richland, Washington, WHC-SD-TI-290.

Luo, S.D., Ku, T.L., Roback, R., Murrell, M., McLing, T.L., 2000. In-situ radionuclide transport and preferential groundwater flows at INEEL (Idaho): decay-series disequilibrium studies. *Geochim. Cosmochim. Acta* **64** (5), 867–881.

Luo, X.Z., Rehkamper, M., Lee, D.C., Halliday, A.N., 1997. High precision Th-230/Th-232 and U-234/U-238 measurements using energy-filtered ICP magnetic sector multiple collector mass spectrometry. *Int. J. Mass Spectrom.* **171** (1-3), 105–117.

Maher, K., DePaolo, D.J., Conrad, M.E., Serne, R.J., 2003. Vadose zone infiltration rate at Hanford, Washington, inferred from Sr isotope measurements. *Water Resour. Res.* **39** (8), 1029–1043.

Maher, K., DePaolo, D.J., Lin, J.C.F., 2004. Rates of silicate dissolution in deep-sea sediment: In situ measurement using U-234/U-238 of pore fluids. *Geochim. Cosmochim. Acta* **68** (22), 4629–4648.

Maher, K., Steefel, C.I., DePaolo, D.J., Viani, B.E., 2006. The mineral dissolution rate conundrum: insights from reactive transport modeling of U isotopes and pore fluid chemistry in marine sediments. *Geochim. Cosmochim. Acta* **70** (2), 337–363.

Murphy, E.M., Ginn, T.R., Phillips, J.L., 1996. Geochemical estimates of paleorecharge in the Pasco Basin—evaluation of the chloride mass balance technique. *Water Resour. Res.* **32** (9), 2853–2868.

Porcelli, D., Swarzenski, P.W., 2003. The behavior of U- and Th-series nuclides in groundwater. In: *Uranium-Series Geochemistry*, vol. 52, pp. 317–361.

Reynolds, B.C., Wasserburg, G.J., Baskaran, M., 2003. The transport of U- and Th-series nuclides in sandy confined aquifers. *Geochim. Cosmochim. Acta* **67** (11), 1955–1972.

Ribeiro, F.B., 1998. Simultaneous diffusion of isotopes from a radioactive series in homogeneous and isotropic solids. *Radiat. Meas.* **29** (1), 9–18.

Richter, F.M., Liang, Y., 1993. The rate and consequences of Sr diagenesis in deep-sea carbonates. *Earth Planet. Sci. Let.* **117** (3–4), 553–565.

Robinson, L.F., Henderson, G.M., Hall, L., Matthews, I., 2004. Climatic control of riverine and Seawater uranium-isotope ratios. *Science* **305** (5685), 851–854.

Serne, J.R., Schaef, H.T., Bjornstad, B.N., Williams, B.A., Lanigan, D.C., Horton, D.G., Clayton, R.E., LeGore, V.L., O'Hara, M.J., Brown, C.F., Parker, K.E., Kutnyakov, I.V., Serne, J.N., Mitroshkov, A.V., Last, G.V., Smith, S.C., Lindenmeier, C.W., Zachara, J.M., Burke, D.B., 2002. *Characterization of uncontaminated vadose zone sediment from the Hanford Reservation—RCRA borehole core samples and composite samples*. Pacific Northwest National Laboratory, Richland, Washington, PNNL-13757-1.

Singleton, M.J., Maher, K., DePaolo, D.J., Conrad, M.E., Dresel, P.E., 2006. Dissolution rates and vadose zone drainage from strontium isotope measurements of groundwater in the Pasco Basin, WA unconfined aquifer. *J. Hydrol.* **321**, 39–58.

Skwarzec, B., 1997. Polonium, uranium and plutonium in the southern Baltic Sea. *Mar. Chem.* **26** (2), 113–117.

Skwarzec, B., Borylo, A., Struminska, D., 2002. ^{234}U and ^{238}U isotopes in water and sediments of the southern Baltic. *J. Environ. Radioact.* **61**, 345–363.

Stonestrom, D.A., White, A.F., Akstin, K.C., 1998. Determining rates of chemical weathering in soils—solute transport versus profile evolution. *J. Hydrol.* **209** (1-4), 331–345.

Tessier, A., Campbell, P.G.C., Bisson, M., 1979. Sequential extraction procedure for the speciation of particulate trace-metals. *Anal. Chem.* **51** (7), 844–851.

Tricca, A., Porcelli, D., Wasserburg, G.J., 2000. Factors controlling the groundwater transport of U, Th, Ra, and Rn. *Proc. Indian Acad. Sci. Earth Planet. Sci.* **109** (1), 95–108.

Tricca, A., Wasserburg, G.J., Porcelli, D., Baskaran, M., 2001. The transport of U- and Th-series nuclides in a sandy unconfined aquifer. *Geochim. Cosmochim. Acta* **65** (8), 1187–1210.

Turkowsky, C., 1969. Electron-microscopic observation of artificially produced alpha-recoil tracks in albite. *Earth Planet. Sci. Lett.* **5** (7), 492–497.

USDOE. 2002. Standardized Stratigraphic Nomenclature for Post-Ringold Formation Sediments within the Central Pasco Basin. U.S. Department of Energy, Richland Operations, Richland, WA., DOE/RL-2002-39.

Vigier, N., Bourdon, B., Turner, S., Allegre, C.J., 2001. Erosion timescales derived from U-decay series measurements in rivers. *Earth Planet. Sci. Lett.* **193** (3–4), 549–563.

White, A.F., Blum, A.E., Schulz, M.S., Bullen, T.D., Harden, J.W., Peterson, M.L., 1996. Chemical weathering rates of a soil chronosequence on granitic alluvium. 1. Quantification of mineralogical and surface area changes and calculation of primary silicate reaction rates. *Geochim. Cosmochim. Acta* **60** (14), 2533–2550.

White, A.F., Brantley, S.L., 2003. The effect of time on the weathering of silicate minerals: Why do weathering rates differ in the laboratory and field? *Chem. Geol.* **202** (3–4), 479–506.

White, A.F., Schulz, M.S., Vivit, D.V., Blum, A.E., Stonestrom, D.A., Harden, J.W., 2005. Chemical weathering rates of a soil chronosequence on granitic alluvium: III. Hydrochemical evolution and contemporary solute fluxes and rates. *Geochim. Cosmochim. Acta* **69** (8), 1975–1996.

Wolery, T.J., Jackson, K.J., Bourcier, W.L., Bruton, C.J., Viani, B.E., Knauss, K.G., Delany, J.M., 1990. Current status of the EQ3/6 software package for geochemical modeling. *ACS Symp. Ser.* **416**, 104–116.

Ziegler, J.F., Biersack, J.P., Littmark, U., 1996. *The Stopping and Range of Ions in Solids*. Pergamon Press, Oxford.